Individualized non-invasive deep brain stimulation of the basal ganglia using transcranial ultrasound stimulation

Ghazaleh Darmani [1,2,8] ✉, Hamidreza Ramezanpour [3,8], Can Sarica [1,2,8], Regina Annirood [1,8], Talyta Grippe[1], Jean-Francois Nankoo[1], Anton Fomenko[2], Brendan Santyr[2], Ke Zeng[1,4], Artur Vetkas[2], Nardin Samuel[2], Benjamin Davidson[2], Alfonso Fasano [1,5,6], Milad Lankarany[1], Suneil K. Kalia[1,2], Samuel Pichardo[7], Andres M. Lozano[1,2,9] & Robert Chen [1,5,6,9] ✉

Transcranial ultrasound stimulation (TUS) offers precise, non-invasive neuromodulation, though its impact on human deep brain structures remains underexplored. Here we examined TUS-induced changes in the basal ganglia of 10 individuals with movement disorders (Parkinson's disease and dystonia) and 15 healthy participants. Local field potentials were recorded using deep brain stimulation (DBS) leads in the globus pallidus internus (GPi). Compared to sham, theta burst TUS (tbTUS) increased theta power during stimulation, while 10 Hz TUS enhanced beta power, with effects lasting up to 40 min. In healthy participants, a stop-signal task assessed tbTUS effects on the GPi, with pulvinar stimulation serving as an active sham. GPi TUS prolonged stop-signal reaction times, indicating impaired response inhibition, whereas pulvinar TUS had no effect. These findings provide direct electrophysiological evidence of TUS target engagement and specificity in deep brain structures, suggesting its potential as a noninvasive DBS strategy for neurological and psychiatric disorders.

Low-intensity transcranial ultrasound stimulation (TUS) has emerged as a promising non-invasive brain modulation technology, offering a level of precision and brain penetration to target deep structures of the brain that traditional non-invasive stimulation methods such as transcranial magnetic stimulation (TMS) and transcranial direct current stimulation (tDCS) cannot achieve[1,2]. TUS has the potential to complement deep brain stimulation (DBS), which requires implanting electrodes into specific brain areas to manage symptoms in various neurological and psychiatric disorders[3].

Studies using TUS have made significant strides in mapping and modulating the functions of cortical and deep brain areas in both animal models and human subjects[4–12]. A substantial body of research has examined the effects of stimulating the motor cortex in rodents, utilizing EMG recordings and observing motor responses[13–16]. These studies suggested that sonication parameters play a role in the direction of neuromodulation (excitation vs. inhibition)[10,11,15,17], and whether TUS effects occur only during stimulation (online effects[6]) or persist beyond stimulation duration after cessation of the TUS (offline

[1]Krembil Research Institute, University Health Network, Toronto, Canada. [2]Division of Neurosurgery, Department of Surgery, University of Toronto, Toronto, Canada. [3]Department of Biology, York University, Toronto, Canada. [4]Department of Psychology, Faculty of Arts and Sciences, Beijing Normal University, Zhuhai, China. [5]Division of Neurology, Department of Medicine, University of Toronto, Toronto, Canada. [6]Edmond J. Safra Program in Parkinson's Disease, Morton and Gloria Shulman Movement Disorders Clinic, Toronto Western Hospital, University Health Network, Toronto, Canada. [7]Department of Radiology, Cumming School of Medicine, University of Calgary, Calgary, Canada. [8]These authors contributed equally: Ghazaleh Darmani, Hamidreza Ramezanpour, Can Sarica, Regina Annirood. [9]These authors jointly supervised this work: Andres M Lozano, Robert Chen.
✉e-mail: ghazaleh.darmani@uhn.ca; robert.chen@uhn.ca

effects[8,12,18]), implying that TUS can induce plasticity. TUS has also been applied in preclinical animal models of neurological disorders[19,20]. For instance, analysis of local field potentials (LFPs) from the motor cortex shows that TUS significantly reduces parkinsonian activity in mice treated with 1-Methyl-4-phenyl-1,2,3,6-tetrahydropyridine (MPTP), suggesting its potential in treatment of Parkinson's disease (PD)[20]. Additionally, in models of temporal lobe epilepsy, TUS has demonstrated the ability to suppress seizures, as evidenced by LFP changes in the hippocampus[21]. Given the promising results from animal studies, TUS has increasingly been explored in clinical settings in conditions such as PD, epilepsy and disorders of consciousness[22–26].

The exact mechanism through which TUS produces modulation of neural elements is incompletely understood, as TUS affects neural activity through a variety of interconnected mechanisms. TUS can alter the physical and electrical properties of neural membranes, notably through membrane deformation that leads to capacitance changes[27–29] and modulating mechanosensitive and specific ion channels[7,30–33], including those in astrocytes that affect glia-neuron interactions by inducing neurotransmitter release[34]. Furthermore, thermal effects from ultrasound can temporarily alter membrane capacitance and affect neuronal conductance and synaptic potentials, offering another mechanism of modulation[35,36].

Although animal studies have provided significant insights into the mechanisms and effects of TUS, direct translation of these findings to human applications remains challenging. Differences in skull size, structure, and acoustic properties between humans and animals influence how ultrasound waves propagate and affect brain activity[1]. Additionally, the parameters for ultrasound stimulation optimized in animals also require careful adjustment and testing in humans to ensure safety and efficacy.

While non-invasive methods have shown that TUS can modulate neural activity and behavior, they often lack the spatial and temporal resolution of invasive methods. This limitation is particularly significant when targeting deep brain areas, as neither fMRI nor EEG can conclusively demonstrate efficient targeting or dynamic changes in neural activity in these regions. This gap limits the potential translational application of TUS in clinical settings, especially for conditions such as movement disorders or epilepsy, where deep structures such as the basal ganglia[37,38] or mesial temporal lobe exhibit pathological oscillations[39].

With this background, our study aims to fill a critical gap by applying TUS to the basal ganglia, specifically to the globus pallidus internus (GPi), to assess its direct neuromodulatory effects on neural activity in DBS-implanted patients, and to investigate its efficacy in modulating behavior in healthy participants. Prior to human application, it was essential to ensure the safety of TUS when applied over DBS leads. To address this concern, we conducted an ex-vivo safety and feasibility experiment with the ultimate goal of employing TUS to stimulate DBS-implanted subjects[40]. Encouragingly, our findings demonstrated no evidence of significant electrode micro motion or thermal rise in the electrode lead during TUS application. In the current study, using the implanted Medtronic Percept device, we employed wireless local field potential recordings in patients with movement disorders (**Experiment I**) to reveal how TUS as a non-invasive technique can specifically modulate LFPs in a deep brain structure such as the GPi.

For assessing the effects of TUS on behavior (**Experiment II**), we sonicated the GPi in healthy individuals and assessed response inhibition behavior using a stop-signal task, which is known to rely on the proper functioning of basal ganglia structures including the GPi and for a comparative analysis, we chose the pulvinar, a posterior nucleus of the thalamus, as a control site, to allow us to discern the specific effects of GPi stimulation on response inhibition. We hypothesized that, similar to TUS of other parts of the basal ganglia[41], TUS of the GPi would impair the inhibitory control in healthy subjects, as reflected by diminished performance (longer stop-signal reaction times) in the stop-signal task, while stimulation of the pulvinar would not produce such effects. This dual approach of studying both disease and healthy brain aims to provide a more comprehensive understanding of direct effects of TUS on neural function and behavior.

Results
The study included two separate experiments, one involving patients with movement disorders (**Experiment I**) and the other involving healthy individuals (**Experiment II**).

Experiment I: TUS of the GPi modulates local field potentials
Experiment I involved three sessions. The first session involved obtaining MRI images for personalized ultrasound simulations. The subsequent sessions, spaced at least one week apart, were allocated to TUS and electrophysiology recordings. Figure 1 provides an overview of the study design and the procedures during an electrophysiology recording session.

The results of acoustic simulations for all patients are illustrated in Fig. 2. We used the same ultrasound exposure (spatial peak pulse average intensity (ISPPA) × sonication duration (SD) × duty cycle (DC)) in both protocols (see Table S2). For tbTUS this was 30 W/cm² (measured in water) × 120 s × 10%, and for 10 Hz TUS, it was 30 W/cm² (measured in water) × 40 s × 30% both resulting in 360 J/cm² to make the neuromodulatory effects comparable. Figure 2A, B shows the transmitted acoustic pressure field and thermal rise in the brain tissue, accounting for skull distortions in one exemplary patient. The maximum temperature rise associated with the 10 Hz TUS was 0.4 °C in the brain, 0.46 °C in the skin, and 0.63 °C in the skull. In contrast, the tbTUS protocol resulted in a maximum temperature rise of 0.16 °C in the brain, 0.25 °C in the skin, and 0.30 °C in the skull, indicating minimal thermal impact (Fig. 2C). Figure 2D demonstrates the extent of transducer repositioning in subject space based on initial simulations, and Fig. 2E shows the average actual distance (unadjusted) and the adjusted distance to the target. The transducer adjustment parameters (Δx, Δy, and Δz) represent spatial corrections made to the transducer's position and orientation to align the ultrasound focus with the intended brain target. These adjustments address initial misalignments due to anatomical variability or setup constraints. Unadjusted distance to target is the distance from the transducer focus to the intended target without considering skull-induced distortions, representing the raw alignment of the focus to the target. Adjusted distance to target is the corrected distance after accounting for skull effects, such as refraction and attenuation, calculated using BabelBrain[42]. The spatial-peak temporal average intensity (ISPTA) values varied between protocols, ranging from 0.75 to 2.1 W/cm² for 10 Hz TUS and from 0.25 to 0.7 W/cm² for tbTUS, due to differences in DC (Fig. 2F). However, ISPPA estimates within the target area based on individual brain characteristics were similar for the two protocols, ranging from 2.5 to 7 W/cm² (Fig. 2G). Both protocols demonstrated mechanical index (MI) values ranging from 0.38 to 0.67 (Fig. 2H). The acoustic simulations predicted that the maximum temperature rise, ISPPA, and MI for both tbTUS and 10 Hz TUS protocols remain within the safety limits established by the FDA[43] guidelines (ISPPA ≤ 190 W/cm²), as well as being consistent with the considerations outlined in the International Transcranial Ultrasonic Stimulation Safety Standards Consortium (ITRUSST) consensus paper (maximal temperature rise anywhere ≤2 °C; MI ≤ 1.9)[44].

Pressure maps derived from ultrasound modeling, superimposed on the MRI image of an example patient (patient S04), highlight the targeting of the DBS lead within the left GPi, as demonstrated in Fig. 2I. Postoperative CT imaging fused with preoperative MRI provides automatically segmented 3D visualizations of the GPi and neighboring structures (GPe, internal capsule, and thalamus), as well as the DBS lead. These elements are superimposed onto the simulated acoustic
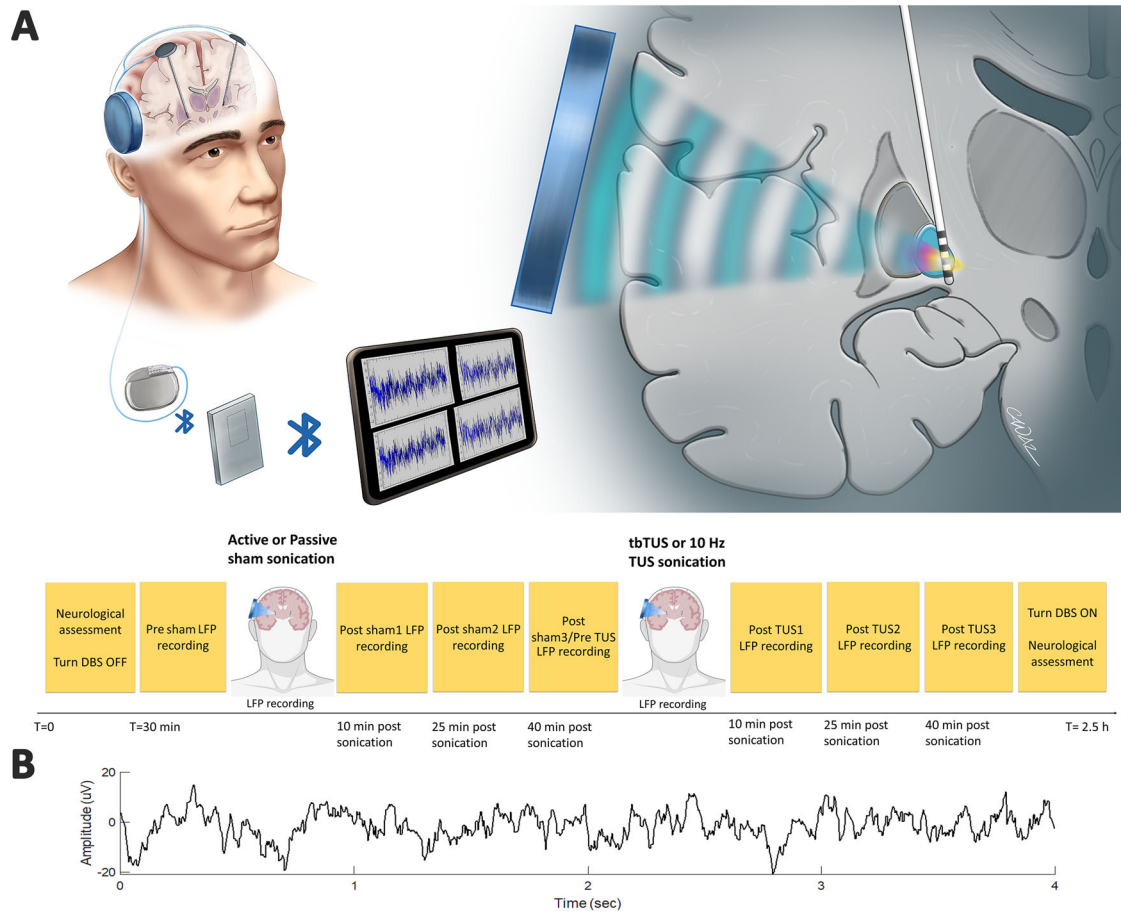
Fig. 1 | Transcranial ultrasound stimulation (TUS) of the GPi in Parkinson's disease and dystonia patients implanted with deep brain stimulation (DBS) devices. A TUS was applied to lead contacts 1 and 9 (contacts are numbered 0-3 on one lead and 8–11 on the other, with 0 and 8 being the deepest ones) for each patient (left and right hemispheres) individually. Local field potentials (LFPs) were recorded wirelessly before, during, and up to 40 min after the application of TUS. The experimental protocol timeline incorporates neurological assessments, baseline LFP recording, TUS application (theta burst transcranial ultrasound (tbTUS), 10 Hz TUS), and sham conditions (active and passive), followed by post-stimulation LFP recordings and a final neurological assessment. A has been printed with permission from © *CC Medical Arts*. B An example of a 4-s long LFP segment recorded wirelessly using the Medtronic Percept device.

focus (Fig. 2J). The size and location of the acoustic focus, in comparison to other structures, including the GPe, GPi, internal capsule, and thalamus, are shown in Fig. 2K.

Once the simulations and modeling were performed, patients participated in two electrophysiology recording sessions. Figure 3A shows that the bilateral GPi-DBS lead locations for all patients (n = 10). During the two electrophysiology sessions, none of the patients reported any discomfort or complications. Furthermore, neurological assessments showed no change in their physical and mental condition before and after TUS applications.

The stimulation was administered in a blinded manner, ensuring that patients were unable to differentiate between sham and active stimulations. Figure 3B shows that the baseline spectral power densities (pre-TUS) for all four conditions (tbTUS, 10 Hz TUS, active sham and passive sham) have a peak in the range of 5–10 Hz, which is consistent with the pattern of the GPi local field potentials at rest in previous studies[45–49]. We found no significant difference among the pre-TUS spectral power densities (Wilcoxon signed-rank test). We next assessed whether the four TUS protocols were able to systematically influence the LFPs in the GPi. Figure 3C–F depicts the distribution of power changes from baseline for each condition individually for data pooled across hemispheres (n = 18 hemispheres, PD patients) and the four timepoints: during TUS (T0), 10 min after TUS (T10), 25 min after TUS (T25), and 40 min after TUS (T40). tbTUS significantly increased the overall power in the 3–30 Hz range (Wilcoxon signed-rank test, p = 0.01) by 7.6% on average (mean ± SEM = 7.6 ± 2.33%). 10 Hz TUS also significantly increased the overall power (Wilcoxon signed-rank test, p < 0.001) by 13% on average (mean ± SEM = 13 ± 2.62%). Neither active sham nor passive sham conditions influenced the spectral power significantly (Wilcoxon sign-ranked test).

While this within-group comparison indicated that only active TUS of the GPi has effects on the neural activity of the GPi, we also performed a between-condition comparison to account for non-specific factors such as the placebo effect or effect of time. This comparison is summarized in Fig. 4. We found that both tbTUS and 10 Hz TUS increased the power significantly compared to the passive sham (Mann–Whitney U-test, p = 0.006, and p < 0.001 respectively), and the active sham (Mann–Whitney U-test, both p < 0.001) stimulation. Changes in the power following 10 Hz TUS were more profound than tbTUS-induced power increase (Mann–Whitney U-test, p = 0.03). Finally, there was no significant difference between the passive sham and active sham conditions (Mann–Whitney U-test, p = 0.45). This between-group comparison, together with the finding that only tbTUS and 10 Hz TUS significantly increase the power in post-stimulation sessions compared to baseline, confirms that we successfully targeted the GPi in this group of PD patients.

Given these results, we then asked whether TUS-induced changes in the overall GPi-LFP power could be manifested more specifically in
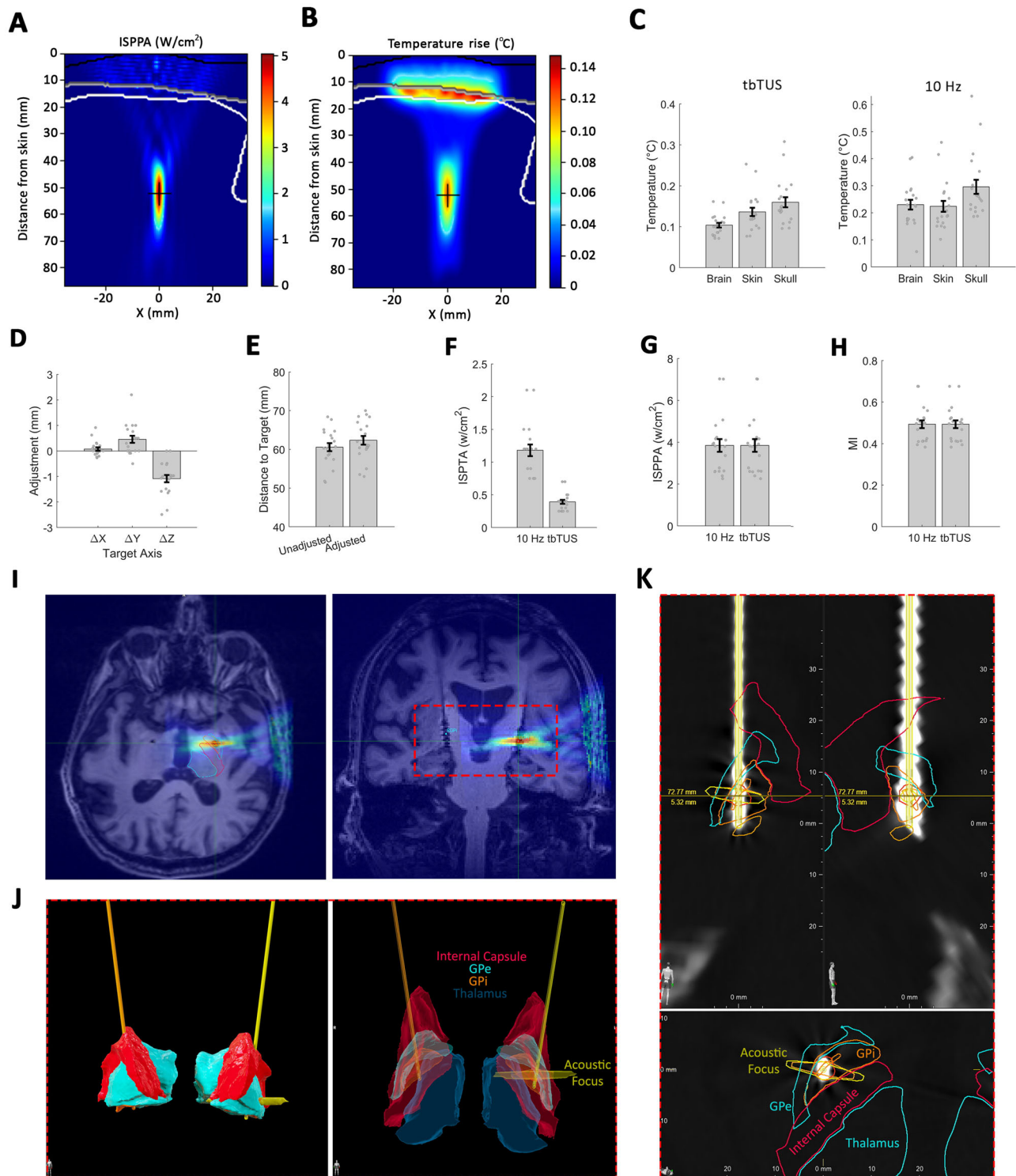
certain frequency bands or time points of measurements. Figure 5 displays percent power changes from baseline in different frequency bands (θ theta [4–7 Hz], α alpha [8–12 Hz], and β beta [13–30 Hz]) after TUS, measured at T0, T10, T25, and T40 minutes post-intervention. We found increased power in most frequency bands and time points following tbTUS or 10 Hz TUS. However, some of the changes did not pass the statistical thresholds due to higher variability (paired t-test or Wilcoxson signed-rank test). Nevertheless, for tbTUS, we found a significant power increase in the theta band (Fig. 5A, B) compared to the passive (Wilcoxon signed-rank test, p = 0.009) and active (paired t-

test, p = 0.03) sham conditions. There was also a significant increase (paired t-test, p = 0.04) and a non-significant trend (paired t-test, p = 0.07) in the beta frequency band only when compared to the passive sham condition. Interestingly, the stimulation-induced pattern was different for 10 Hz TUS, where most of the statistically significant results were found in the beta frequency band and outlasted the stimulation duration more consistently. Figure 5C shows that 10 Hz TUS-induced increase in beta power compared to passive sham stimulation that lasted up to 40 min post-stimulation (paired t-tests, T0: p = 0.004, T10: p = 0.002, T25: p = 0.0003, T40: p = 0.03). Similarly, we found

Fig. 2 | Acoustic simulation estimates of the acoustic pressure distribution and temperature changes in the GPi-DBS patients. A Spatial intensity distribution for patient S10, with red indicating the highest intensity and blue the lowest. The ultrasound beam's focal point was located within the GPi. **B** Estimated temperature rise in different brain tissues for the same patient S10, with the highest temperature rise observed at the skull due to absorption and heating effects from the ultrasound energy. In both simulations, the transducer was positioned externally at the top, with the skull's outline and ultrasound waves shown penetrating through to the target area. **C–H** Comparative analysis of simulated ultrasound parameters for two sonication protocols, theta burst transcranial ultrasound (tbTUS) and 10 Hz TUS. **C** Estimated temperature in the skin, skull, and brain for both protocols (n = 20 hemispheres). **D** Transducer adjustments in subject space along the x, y, and z axes in mm to compensate for ultrasound beam deviations based on BabelBrain simulation results (n = 20 hemispheres). **E** Sonication depth based on BabelBrain simulation results compared to the unadjusted distance from the transducer to the target location (n = 20 hemispheres). **F–H** In situ intensity values of Spatial Peak Temporal Average (ISPTA), Spatial Peak Pulse Average (ISPPA), and Mechanical Index (MI) for both protocols. Note that 10 Hz TUS results in higher ISPTA values than tbTUS (n = 20 hemispheres). Data are presented as mean ± standard deviation. **I** Pressure maps derived from ultrasound modeling superimposed on the MRI image of patient S04, highlighting the targeting of the DBS lead within the left GPi. **J** Postoperative CT imaging fused with preoperative MRI, featuring automatically segmented 3D visualizations of the GPe (turquoise), GPi (orange), internal capsule (red), thalamus (navy blue), and the DBS lead. These elements are superimposed onto the simulated acoustic focus (yellow) using BrainLab software. **K** The in-line view of the DBS lead artifact for the same patient (S04), along with the simulated acoustic focus (with the epicenter outlined in red, orange, and yellow), is shown. The lower part of (**K**) illustrates the size and location of the acoustic focus in comparison to other structures, including the GPe, GPi, internal capsule, and thalamus.

long-lasting changes in the power relative to the baseline when we compared the 10 Hz TUS and the active sham protocol (Fig. 5D). There was a significant increase in beta power at T10 (paired t-test, p = 0.01) and T25 (paired t-test, p = 0.003) and non-significant changes at T0 (paired t-test, p = 0.09) and T40 (paired t-test, p = 0.06). There was also a significant increase in power in the theta band at T40 when we compared 10 Hz TUS with the passive sham condition (paired t-test, p = 0.03). We also compared tbTUS and 10 Hz TUS directly and found significantly larger power increases in the theta band for tbTUS (Fig. S2) compared to 10 Hz TUS (t-test, p = 0.0082). Additionally, there was a significant difference in beta power increases at T25 (paired t-test, p = 0.021). Altogether, these results indicate that tbTUS and 10 Hz TUS protocols have distinct effects on neural activity within the GPi. Notably, TUS of the GPi in the dystonia patient with GPi-DBS implants also increased overall power (Fig. S3), similar to the effects observed in PD patients. The power changes were most prominent in the alpha and beta bands (Fig. S4). Further research is needed to determine whether these findings can be generalized to a larger population of dystonia patients.

PD patients exhibit diverse symptoms, which may lead to unique effects of TUS for different subpopulations. To explore this, we analyzed power changes across various frequency bands in two distinct subgroups of PD patients: the akinetic-rigid group (patients 4, 5, 6, 7, 8, 9) and the tremor-dominant group (patients 1, 2, 3). As shown in Fig. S5, we observed a significantly higher theta and alpha power (p = 0.04, p = 0.04, two-sample t-test) in the akinetic-rigid compared to the tremor-dominant group in response to the 10 Hz TUS compared to the passive sham condition (data pooled across four timepoints). This result is particularly noteworthy, as increased power in the 4–10 Hz range within the globus pallidus has been associated with symptom improvement in PD patients[45]. These findings may suggest that 10 Hz TUS may offer greater therapeutic benefits for akinetic-rigid PD patients compared to tremor-dominant patients in this small cohort.

Studies have suggested that TUS-induced neural effects might depend on certain neurotransmitter systems[50]. Therefore, the interaction between dopaminergic medication dosage and the efficacy of TUS of the GPi in PD patients may reveal information about how TUS may work in humans. Hence, we assessed whether the neural effects of TUS of the GPi were modulated by the dose of dopaminergic medications as indexed by the Levodopa Equivalent Daily Dose (LEDD). Compared to the two sham conditions (Fig. 6A, B), we found a significant positive correlation between LEDD and the tbTUS-induced total power changes in the GPi during stimulation (tbTUS - Passive Sham: r = 0.68, and p = 0.001; tbTUS - Active Sham: r = 0.66, and p = 0.002), suggesting that the neural effects of tbTUS were related to the dopaminergic state of the patient. Similarly, we found significant positive correlations between LEDD and tbTUS-induced neural changes at T10, T25 and T40 (Table S1). Also, there was a significant positive

correlation between LEDD and the 10 Hz TUS-induced total power changes during stimulation, but only when compared to the passive sham (r = 0.63, and p = 0.004, Fig. 6C) and not when compared to the active sham condition (r = 0.35, and p = 0.14, Fig. 6D). The correlation between LEDD and 10 Hz TUS-induced changes after cessation of sonication (measured at T10, T25, and T40) was also significant (Table S1). We did not find any significant correlations between LEDD and power changes in the active sham compared to the passive sham condition during or after cessation of the stimulation (Table S1). These findings underscore the necessity of considering individual pharmacological profiles when administering ultrasound stimulation in PD management.

In contrast to positive correlations with the LEDD, no correlation was observed between power changes with tbTUS or 10 Hz TUS and the Movement Disorder Society Unified Parkinson's Disease Rating Scale (MDS-UPDRS) scores during (left panels in Fig. 6A–D) or following TUS application at T10, T25, and T40. It should be noted that the MDS-UPDRS scores were in the ON-medication state and were the latest evaluations from routine clinical assessments conducted up to a few months before this study.

Finally, we examined the correlations between the ISPPA (as an estimate of exposure) and power changes across various conditions and time points but found no significant correlations. Although no exposure-related changes in the LFPs were observed—possibly due to small individual variations in the ultrasound exposure—future studies would benefit from developing an exposure-response curve for the tbTUS and 10 Hz TUS protocols.

Experiment II: causal effects of TUS of deep brain regions on behavior are location specific

In this experiment, effects of TUS of the GPi on response inhibition behavior was assessed in healthy participants. Pulvinar, a posterior nucleus of the thalamus served as a control site. Sonication of the GPi and pulvinar was performed in separate sessions. Each stimulation session consisted of three blocks of the stop-signal task: one baseline block, and two blocks following the application of tbTUS (Fig. 7A) to the GPi or pulvinar. The schematic of the stop-signal task is shown in Fig. 7B.

The results of acoustic simulations for all participants in this experiment are illustrated in Fig. 8. The maximum temperature rise associated with GPi stimulation was 0.22 °C in the brain, 0.61 °C in the skin, and 0.85 °C in the skull. The maximum temperature rise associated with pulvinar stimulation was 0.30 °C in the brain, 0.69 °C in the skin, and 0.91 °C in the skull (Fig. 8A). Figure 8B demonstrates the extent of transducer repositioning in subject space based on initial simulations. The MI values ranged from 0.32 to 0.72 for the GPi and 0.39 to 0.77 for the pulvinar (Fig. 8C). Figure 8D, E suggests the ISPPA estimates within the target area ranged from 1.6 to 8 W/cm² for the GPi
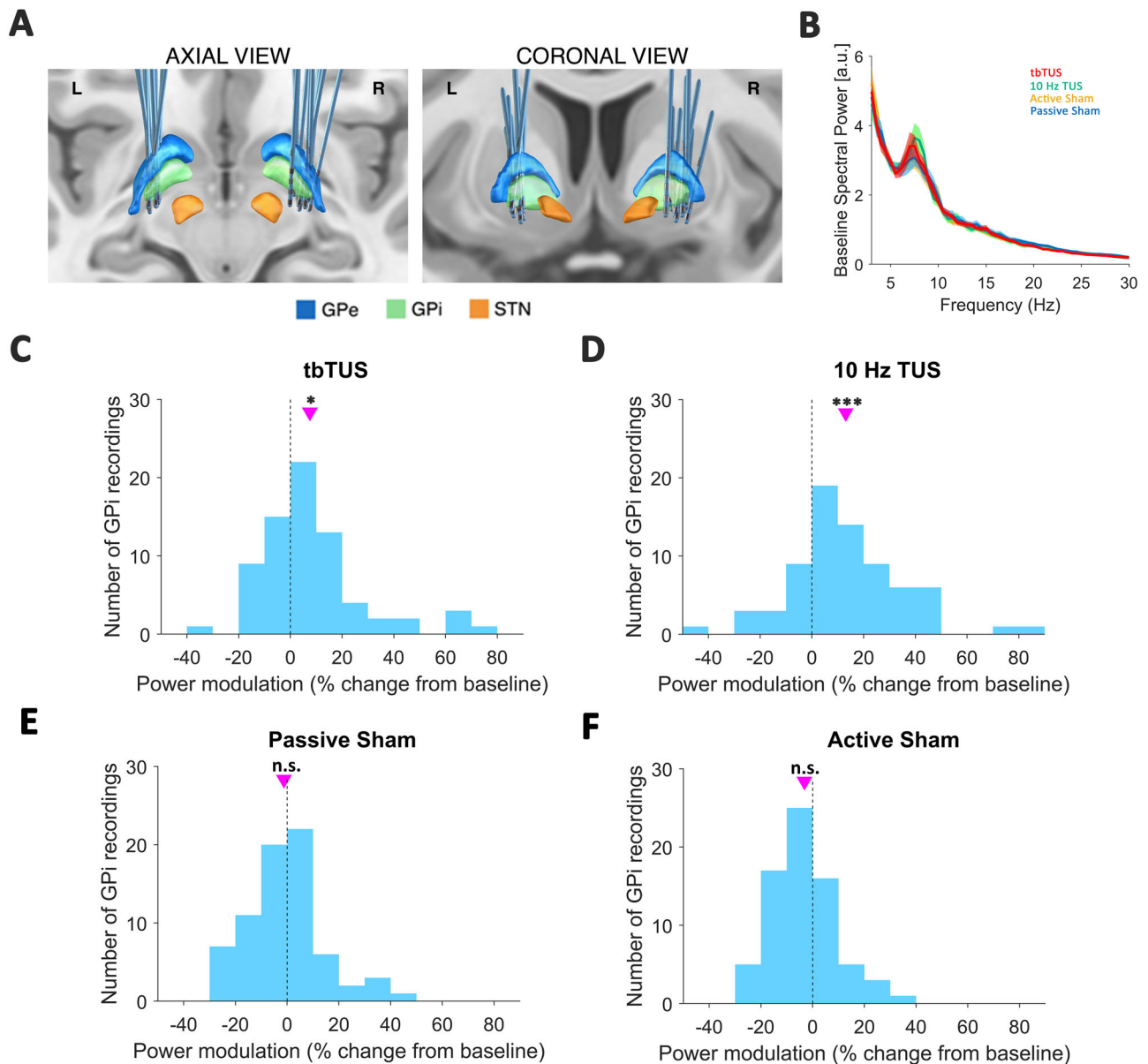
Fig. 3 | DBS lead localization and power changes from baseline for all TUS protocols. A The localizations of the DBS leads in the GPi (n = 9 PD patients, n = 1 dystonia patient) demonstrated in both axial and coronal brain views. **B** Comparison of baseline spectral power across the tbTUS, 10 Hz TUS, active sham, and passive sham conditions, indicating no significant differences in total baseline LFP power spectra (3–30 Hz) prior to the application of TUS (Wilcoxon signed-rank test). Shaded areas represent the standard error of the mean. **C–F** Histograms represent the total percentage change in spectral power (3–30 Hz) from baseline following each TUS protocol. The data has been pooled across all 18 hemispheres (n = 9 PD patients) and at four different time points post-TUS. While tbTUS (**C**), and 10 Hz TUS (**D**) significantly increased the overall power from baseline (tbTUS: p = 0.01, 10 Hz TUS: p = 7E-06), passive sham and active sham TUS (**E**, **F**) had no significant effects (passive sham: p = 0.06, active sham: p = 0.8). Statistical Significance was tested by a two-sided Wilcoxon signed-rank test with Bonferroni adjustment. Asterisks indicate statistical significance (*p < 0.05, ***p < 0.001) and the pink downward-pointing triangles indicate the mean of the distribution. The vertical dashed line at 0% denotes the baseline level for reference.

and 2.3 to 9 W/cm² for the pulvinar; In addition, the ISPTA estimates within the target area ranged from 0.2 to 0.85 W/cm² for the GPi and 0.25 to 0.95 W/cm² for the pulvinar. These simulations predicted that the maximum temperature rise across the entire duration of TUS, MI and ISPPA for both areas were well below the safety guidelines[43,44]. Figure 8F shows the average actual distance (unadjusted) and the adjusted distance to target the GPi and pulvinar, using BabelBrain software to compensate for skull energy losses and beam distortions. Figure 8G shows the acoustic pressure maps superimposed on MRI images of a representative subject, highlighting the target areas: GPi and pulvinar.

While tbTUS of the GPi significantly increased the stop-signal reaction times (SSRTs) in both post-TUS blocks (paired t-test, post1: p = 0.03, post2: p = 0.01) compared to pre-TUS block (Fig. 9A), tbTUS of the pulvinar had no effects on the SSRTs (p > 0.05, paired t-test, Fig. 9C). There were also no significant effects on the go trial reaction times (paired t-test) for both GPi or pulvinar targets (Fig. 9B, D). Additionally, there was a significant difference between the baseline-normalized SSRT changes (post - pre) for GPi and pulvinar (p = 0.04, two-sample t-test; Fig. 9E). We found no significant difference in the go trial reaction times between the two regions (p = 0.86, two-sample t-test, Fig. 9F). For
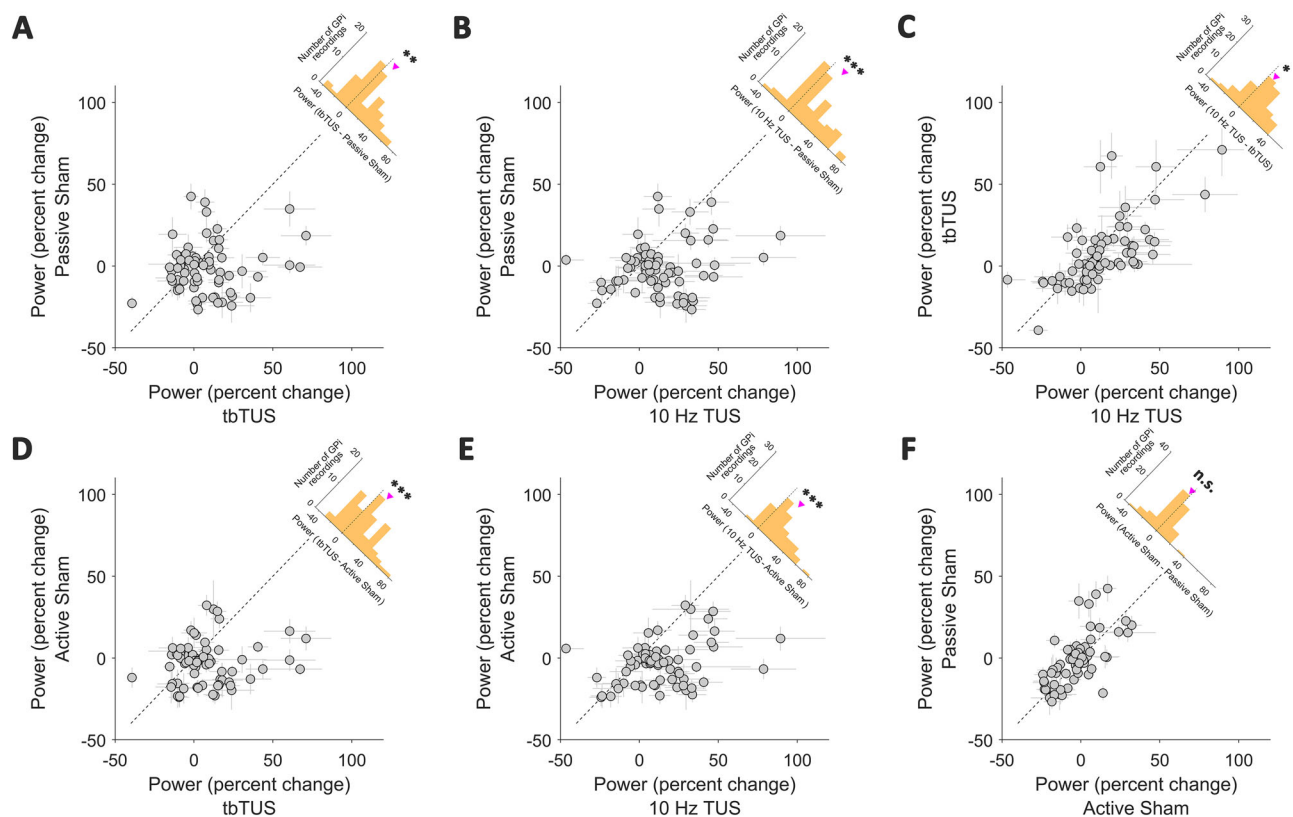
Fig. 4 | Comparative analysis of spectral power changes across different stimulation protocols. This collection of scatter plots, labeled (**A–F**), illustrates the percent change in power for various stimulation conditions. Both tbTUS and 10 Hz TUS increased the power significantly compared to the passive sham (Mann–Whitney U-test, p = 0.006, and p = 4.55E-06 respectively), and the active sham (Mann–Whitney U-test, p = 0.0003, and p = 3.57E-07 respectively) stimulation. Changes in the power following 10 Hz TUS were more profound than tbTUS-induced power increase (Mann–Whitney U-test, p = 0.03). Finally, there was no significant difference between the passive sham and active sham conditions (Mann–Whitney U-test, p = 0.45). In (**A–F**), p-values were adjusted by Benjamini-Hochberg procedure to control FDR. Each dot represents an individual hemisphere/timepoint measurement (n = 18 hemispheres, 4 different time points), and error bars indicate the standard error of the mean of power across the entire frequency range of 3 to 30 Hz. Superimposed histograms on the right side of each plot reveal the distribution of changes, with the inverted triangle denoting the mean of each distribution. The dashed line in each plot marks the zero point, serving as a baseline for comparison. Significant differences between the means of each histogram are highlighted with asterisks, where * denotes p < 0.05, ** signify p < 0.01, and *** indicate p < 0.001. These differences are measured in terms of power changes between each pair of stimulation protocols.

these comparisons, data from the first and second post- measurements were pooled.

Discussion

The integration of TUS with wireless intracranial recordings from electrodes implanted for DBS offers a promising approach to study the direct effects of TUS in humans. Using this technology, we investigated the impact of individualized TUS of the basal ganglia by recording LFPs directly from the GPi in patients with movement disorders, alongside behavioral experiments in healthy subjects. We found that both tbTUS and 10 Hz TUS protocols significantly increased overall GPi LFP power. In addition to the physiological effects (Experiment I), we also observed that tbTUS of the GPi, but not the pulvinar, disrupts response inhibition in healthy subjects (Experiment II), lending further support to the notion that TUS is able to modulate neural circuits in a spatially precise manner.

Evidence for target engagement

The modulation of LFP power across different frequency bands with tbTUS and 10 Hz protocols, with the absence of power changes in both sham conditions, represents the first evidence of target engagement. The second piece of evidence comes from our behavioral experiment indicating that tbTUS applied to the GPi of healthy individuals influenced behavior in a stop-signal

task while sonication of the pulvinar as a control site had no effects on behavior.

We observed that increases in GPi LFP power were larger with 10 Hz stimulation compared to tbTUS (10 Hz TUS_{mean} − $tbTUS_{mean}$ = 5.56, Fig. 4C), despite using an equal ultrasound exposure ($I_{SPPA} \times SD \times DC$) for both protocols. A similar phenomenon, wherein the effect size or direction of neuromodulation changes with varying PRFs and DCs while maintaining a constant ultrasound exposure, has been demonstrated in animal models[11], as well as in studies in healthy human participants[51,52].

Previous studies have shown that tbTUS applied to the primary motor cortex (M1) can increase corticospinal excitability[51]. In contrast, the 10 Hz protocol applied to the M1 has been shown to decrease corticospinal excitability in healthy humans[41]. M1 and GPi are distinct in their cellular composition, size, connectivity, and functions. Moreover, the relationship between LFP power changes and neural activity is intricate and context-dependent. Therefore, increases in GPi LFP power in the current study may not be directly translated to changes in the excitability of neurons in the M1 as observed in previous studies. This is further supported by previous imaging studies which have demonstrated that applying the same TUS protocol to two different regions may yield different outcomes depending on the state, as well as the structural and functional properties of the targeted region and its associated networks[8,53].
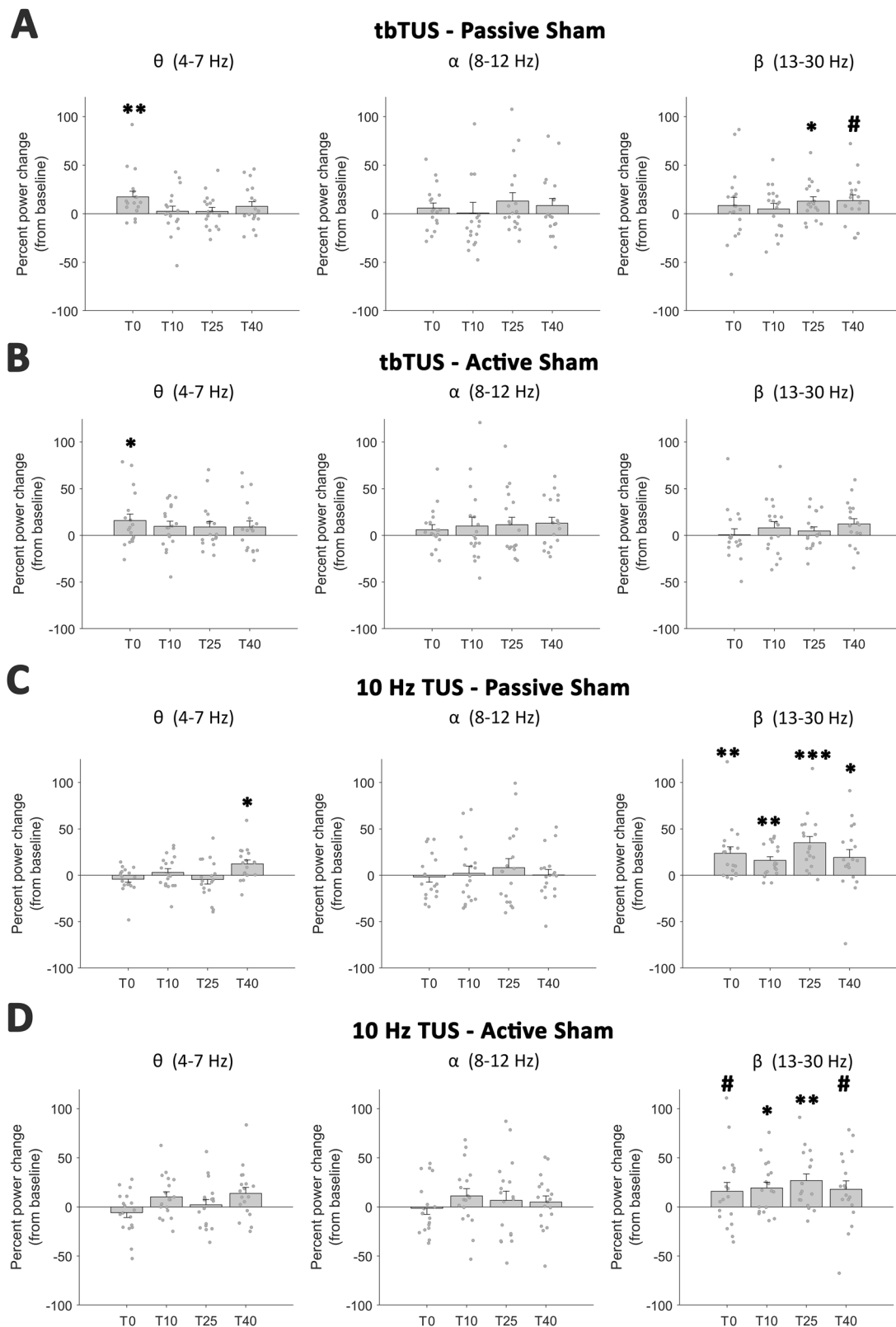
Nevertheless, the change in corticospinal excitability measured through TMS-motor evoked potentials (MEPs) and increase in oscillatory power in the current study highlight different aspects of neural processing can be affected by TUS. To accurately determine whether the observed modulations in LFP power reflect excitation or inhibition, direct measurements from single cells, often performed invasively in animal models, are required.

To better delineate the effects of TUS and distinguish between the two protocols, we examined the LFP power changes at different time points in different frequency bands. We found a more profound and consistent increase in the theta band power during tbTUS (Fig. 5A, B), and stronger beta band increase following 10 Hz TUS which lasted up to 40 min after completion of the ultrasound stimulation (Fig. 5C, D). These results suggest that the stimulation effects were indeed

Fig. 5 | Percent power change from baseline in distinct frequency bands following TUS of GPi. This figure displays the changes in spectral power within different frequency bands (θ theta [4–7 Hz], α alpha [8–12 Hz], and β beta [13–30 Hz]) from baseline after transcranial ultrasound stimulation (TUS), measured at T0, T10, T25, and T40 minutes post-intervention (n = 18 hemispheres). The error bars represent the standard error of the mean. The panels depict comparisons between TUS and sham conditions: **A** shows tbTUS - Passive Sham with significant increase in θ power at T0 (p = 0.009, Wilcoxon signed-rank test) and β power at T25 (p = 0.04, paired t-test), as well as a non-significant trend (denoted by #) towards increase in β power at T40 (p = 0.07, paired t-test). **B** illustrates tbTUS - Active Sham with significant increase in θ power at T0 (p = 0.03, paired t-test); **C** represents 10 Hz TUS -

Passive Sham, indicating significant increase in β power at T0, T10, T25, and T40 (p = 0.004, p = 0.002, p = 0.0003, and p = 0.03 respectively, paired t-test), as well as in θ power at T40 (p = 0.03, paired t-test) and **D** displays 10 Hz TUS - Active Sham with significant increase in β power at T10, and T25 (p = 0.01, and p = 0.003 respectively, paired t-test), as well with non-significant increase in β at T0 and T40 post-TUS (p = 0.09, and p = 0.06 respectively, paired t-test). Asterisks denote levels of statistical significance (*p < 0.05, **p < 0.01, ***p < 0.001), and hash signs (#) indicate statistical trends (non-significant changes in the range of 0.05 <p < 0.1)). In each frequency band, p-values were adjusted by Benjamini-Hochberg procedure to control FDR. All statistical tests were two-sided.

parameter-specific, with the 5 Hz and 10 Hz TUS protocols eliciting distinct effects on neural activities within the GPi likely due to different neuromodulatory mechanisms triggered by each protocol.

While our methodology was carefully planned and the transducer was positioned and oriented with high precision during the session, it is important to acknowledge the potential limitations associated with neuronavigation using optical tracking, which may introduce a tracking error of 2–3 mm[54–56]. This level of variability, could impact precise engagement with small targets such as a single DBS lead contact. Indeed, neuronavigation error might be one of the reason that when we analyzed the data from individual contact pairs (e.g., 0–3, 0–2, 1–3), we did not find any significant differences between them. Additionally, the focus of the ultrasound beam is sufficiently large (4.7 mm width) that, when combined with navigation errors, precise targeting of a specific lead contact becomes highly challenging. To address this, we averaged the power spectral densities (PSDs) contact pairs to reduce noise effects when reporting the data. Despite this potential misalignment, our LFP readouts clearly demonstrate TUS-induced modulation in the GPi compared to sham conditions, underscoring the effectiveness of our approach (notably, LFP signals can be recorded up to 5 mm radially around the lead). Future improvements could be achieved by exploring alternative methods to better stabilize the devices during experiments[57,58].

Role of dopaminergic medication and tailoring TUS parameters for optimized therapeutic outcomes

There is mounting evidence that TUS interacts with various neurotransmitter systems such as GABA, serotonin, and dopamine[9,50,53,59]. For example, in Parkinson's disease, characterized by the progressive degeneration of dopaminergic neurons, studies suggest that the neuromodulatory effects and clinical benefits of TUS are more pronounced when patients are in the ON medication state compared to the OFF medication state[22,26]. We found a positive correlation between increased LFP power and LEDD following tbTUS, compared to active and passive sham conditions, thereby expanding previous findings regarding the role of dopamine in modulating TUS efficacy. However, for the 10 Hz TUS protocol, this positive correlation was evident only when compared to the passive sham. Patients with higher LEDD are likely further along in their disease progression, as they require higher medication doses. This suggests that the positive correlation with LEDD may reflects a neuromodulatory effect of TUS that is influenced by the dopaminergic state or disease severity.

In PD patients in the medication-OFF state, subthalamo-pallidal networks typically exhibit oscillations below 30 Hz, driven primarily by two effects: (1) low-frequency oscillations at 4–10 Hz with the STN leading GPi, possibly associated with resting tremor; and (2) beta activity where GPi phase leads STN. With dopaminergic medications, oscillations below 30 Hz are significantly reduced[60], while theta and alpha band (low-frequency) activities exhibit a substantial increase following levodopa intake or DBS, correlating with the alleviation of motor symptoms in patients with PD[45,60–62]. Similar to levodopa and DBS, tbTUS significantly increased theta power during stimulation

compared to both sham conditions. Although there was an increasing trend observed at other time points in the theta band and throughout all time points in the alpha band, these trends did not reach statistical significance. These effects were specific to the 5 Hz stimulation (tbTUS) and were not observed with the 10 Hz stimulation. The enhancement of beta band activity, potentially associated with increased motor symptoms in PD, was evident with 10 Hz stimulation, where beta power increased significantly during sonication and remained elevated throughout the study visit compared to both sham groups. This effect was not observed with tbTUS protocol; the only significant effect occurred after 25 min of tbTUS compared to the passive sham, with no notable increase compared to the active sham condition.

Increased beta activity is often associated with worsened motor symptoms in Parkinson's disease, raising questions about the suitability of 10 Hz TUS for symptom suppression. But Clinical scores or behavioral changes were not directly assessed in this study, as the focus was on target engagement and electrophysiological effects. General neurological safety evaluations revealed no adverse effects or worsening of symptoms, but subtle changes may have been undetectable within the experiment's timeframe. Additionally, no correlation was found between power changes and MDS-UPDRS scores, which were taken from routine clinical assessments before the study. As higher MDS-UPDRS scores reflect more severe or advanced Parkinson's disease, the lack of correlation suggest that TUS effects may be independent of overall disease severity. Future investigations should directly measure clinical and behavioral outcomes immediately before and after TUS applications to clarify these effects.

Could the observed increase in beta power with 10 Hz protocol be due to the gradual wearing off of the levodopa effects near the end of the study visit? At least three factors argue against this suggestion: (1) There was no significant difference between baseline powers for the tbTUS and 10 Hz TUS compared to the two sham conditions, and the sham condition was always tested before the active TUS conditions (Fig. 3B); (2) Since LFP may be affected by the timing of dopaminergic medications in PD patients, we scheduled all patients study visits such that they took their medications at the beginning of the experiment (according to their routine schedule) and we designed the study to be as brief as possible, with a duration under two and half hours. (3) Additionally, the changes observed with 10 Hz TUS were not seen with tbTUS, even though both were administered within the same time frame. Therefore, the neuromodulatory effects of TUS likely cannot be accounted for by changes in medication effects during the study. Nevertheless, testing patients in a medication-off state would provide further insight into the interaction between TUS effects and dopamine signaling, and future studies should explore this possibility.

Altogether, the differential effects of the tbTUS and 10 Hz TUS on the GPi and their dependencies on the dopaminergic state, suggest the potential for applying specific TUS frequencies to optimize treatment effects tailored to the unique electrophysiological characteristics of different brain regions in future clinical studies.
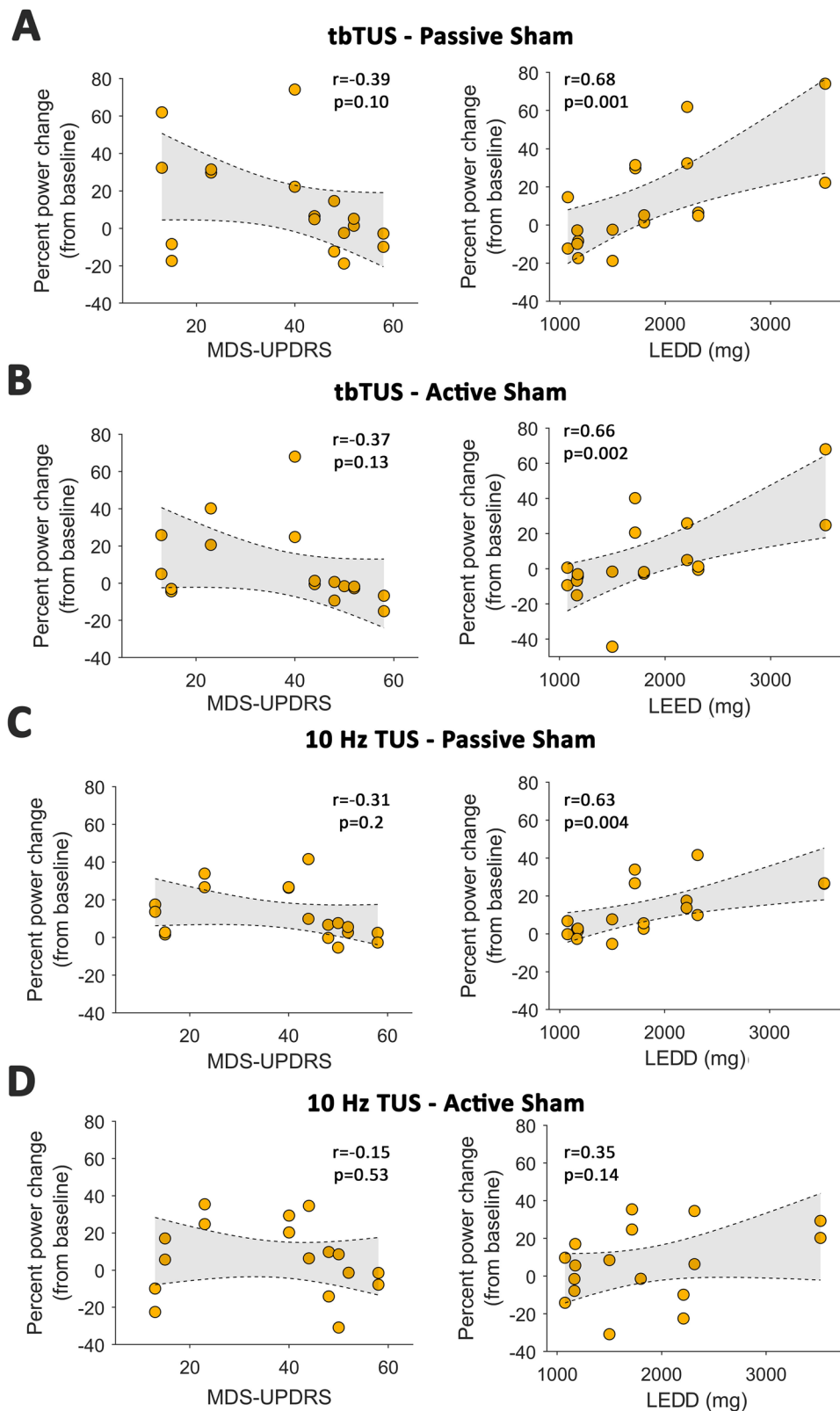
Fig. 6 | Correlation analysis of percent power change from baseline with MDS-UPDRS scores and LEDD dosage following TUS protocols. This figure displays scatter plots examining the relationship between percent power change from baseline (n = 18 hemispheres) and clinical as well as pharmacological variables across different TUS protocols. Each panel presents Pearson correlation values (r) and associated significance levels (p-values), analyzing the potential link between changes in spectral power and either MDS-UPDRS scores or LEDD (Levodopa Equivalent Daily Dose) in milligrams (mg). **A, B** show the correlations for tbTUS (theta burst TUS) with Passive and Active Sham respectively, while **C, D** illustrate the same for 10 Hz TUS with Passive and Active Sham, respectively. The left graphs of each panel correspond to correlations with MDS-UPDRS, and the right graphs with LEDD dosage. Notably, significant correlations are observed in the right graphs of (**A, B, C**), suggesting a relationship between LEDD dosage and spectral power change in these conditions. The shaded areas around the dotted line represent the 95% confidence intervals for the regression estimates.
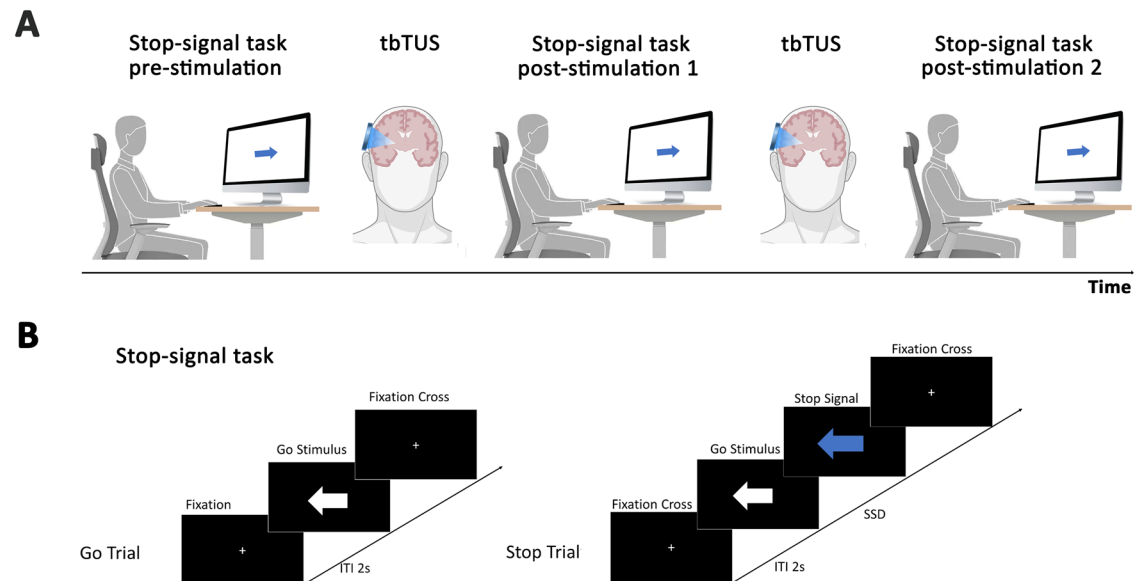
Fig. 7 | Causal effects of the TUS of the GPi and pulvinar on inhibitory control behavior. A Schematic of the behavioral study design: Fifteen healthy participants performed the task three times in each session: before sonication, after the first round of sonication, and after the second round of sonication. Part of this figure has been Created in BioRender. Ramezanpour, H. (2025) https://BioRender.com/p29x980.

B Schematic of the stop-signal task used to measure inhibitory control. In Go trials, participants respond to a go stimulus, while in stop trials, they attempt to inhibit their response upon seeing a stop signal, with a stop-signal delay (SSD) adjusted to create a 50% successful stop rate. ITI inter trial interval.

TUS-induced changes in behavior are target specific

A few studies have applied TUS to deep brain structures and used behavioral outcomes or indirect measures of neural activity to assess the effects of TUS in healthy human subjects[6,53,63,64]. In order to make a broader conclusion on the efficacy and functionality of this newly developed technique, we conducted a behavioral experiment in healthy participants, wherein we applied tbTUS to the GPi while assessing behavioral changes using a stop-signal task−a paradigm that measures response inhibition and has been shown to be reliant on basal ganglia functions[41,65–67]. Moreover, selected the pulvinar for active sham stimulation. Given its proximity to the GPi and its lack of known involvement in inhibitory control, the pulvinar serves as an appropriate control site, allowing for accurate assessment of TUS location specificity. We found that tbTUS of the GPi, and not the pulvinar, impaired the inhibitory control in healthy subjects, as reflected by longer stop-signal reaction times (SSRTs) in the stop-signal task. Our findings are consistent with a previous study which showed that 10 Hz TUS of the subthalamic nucleus (STN) or anterior putamen, two other basal ganglia regions, can also disrupt stopping behavior[41]. In the same study, TUS of the posterior putamen did not affect SSRTs. Altogether, these results provide evidence of the target specificity of TUS neuromodulation. The ability to efficiently modulate deep brain areas not only has therapeutic implications but could also enable the exploration of the causal roles of deep brain regions in sensory, cognitive, and motor functions, which has not been possible with other non-invasive brain stimulation techniques. However, we acknowledge that the behavioral findings from this experiment in healthy participants may not necessarily generalize to individuals with movement disorders.

Future directions

While previous TUS studies in humans were limited to recordings of cortical and corticospinal activities and imaging techniques such as EEG, EMG, MEG, and fMRI to assess TUS effects[2,24], this study expands our capability to directly evaluate circuit function during and after TUS using DBS leads in deep brain structures. This is of significant translational importance, given the broad utilization and investigation of DBS across diverse conditions, including movement disorders, epilepsy, pain, Alzheimer's disease and psychiatric conditions. The methodology presented in this paper not only enables assessment of TUS effects on circuit function via LFPs across all DBS indications, but also could lead to the developing more efficient protocols to restore function in neurological and psychiatric disorders.

Methods

The study included two separate experiments, involving patients with movement disorders (**Experiment I**) and healthy individuals (**Experiment II**). Both experiments were approved by the Research Ethics Board (REB) of University Health Network (UHN) and conformed to the latest version of the Declaration of Helsinki.

Experiment I: neural effects of TUS

Participants. Ten patients (nine PD patients and one dystonia patient) with GPi-DBS implants (ClinicalTrials.gov identifier NCT06232629) participated in this experiment. Informed consent was obtained from all participants. No statistical method was used to predetermine the sample size. See Table 1 for patients' demographics. A known sex disparity exists in DBS surgeries for PD, with women accounting for only 30% of all procedures[69]. This disparity was also evident in the current study, manifesting as a sex bias. While currently there is no evidence of differential effects of TUS based on sex, future studies might aim for a more balanced sex distribution. Patients were recruited who were on stable dopaminergic medications and had bilateral GPi-DBS with a commercial IPG capable of both stimulation and recording (Percept PC, models 3387 and B33015; Medtronic Inc.). Patients were included regardless of age, sex, or disease severity and covered both new DBS implants and older systems upgraded with the Percept PC battery. Participants were excluded if they had any neurological condition other than PD, significant psychiatric disorders, a MoCA score below 22, cardiac or other neurological implants, a history of intracranial lesioning or the implantation of more than two leads, serious illness, infection, pregnancy, or damaged lead contacts.
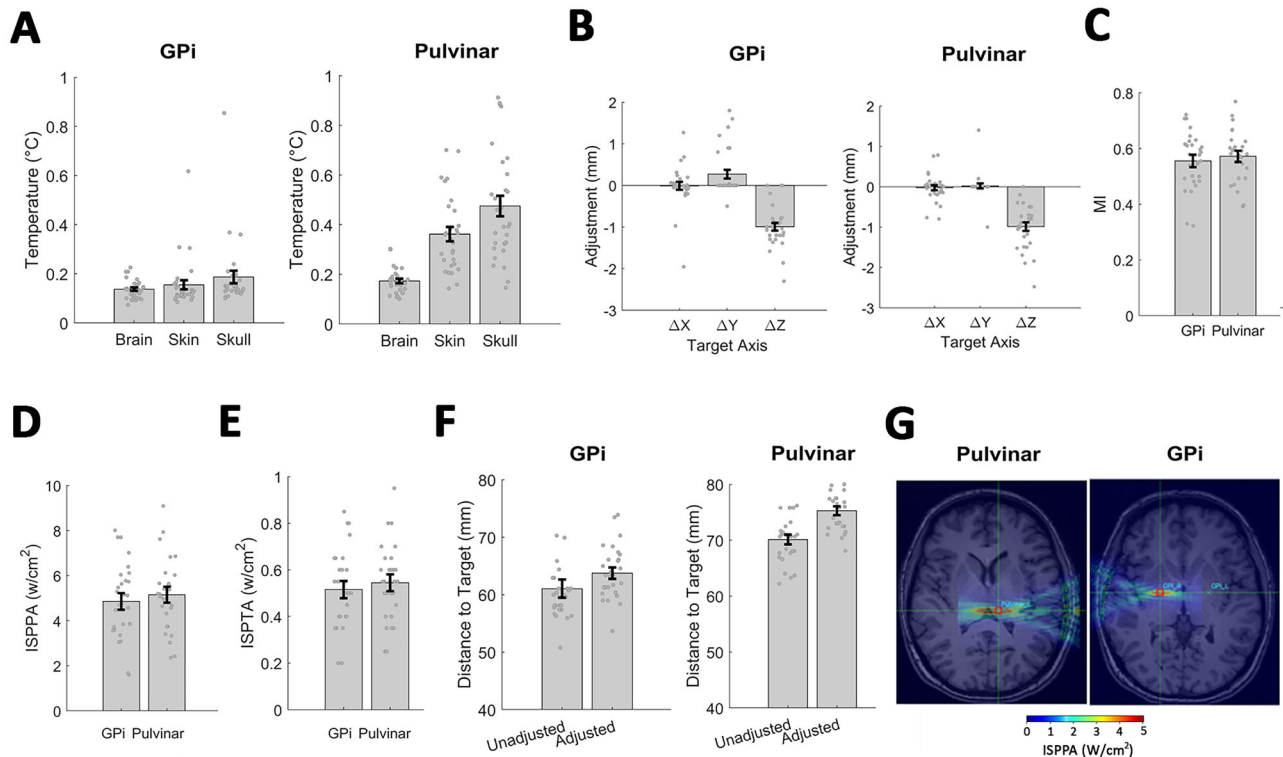
Fig. 8 | Acoustic simulation estimates of the acoustic pressure distribution and temperature changes in the healthy participants in Experiment II. A Estimated temperature change for both targets. (GPi: n = 30 hemispheres, Pulvinar: n = 29 hemispheres) **B** Transducer adjustments in subject space along the x (ΔX), y (ΔY), and z (ΔZ) axes in mm to compensate for ultrasound beam deviations based on BabelBrain simulation results (GPi: n = 30 hemispheres, Pulvinar: n = 29 hemispheres). **C–E** In situ intensity values of the Mechanical Index (MI), Spatial Peak Pulse Average (ISPPA), and Spatial Peak Temporal Average (ISPTA) for both targets (GPi: n = 29 hemispheres, Pulvinar: n = 29 hemispheres). **F** The average actual distance and the adjusted distance to target GPi (n = 30 hemispheres) and Pulvinar (n = 30 hemispheres) after corrections for skull energy losses. Error bars indicate the standard error of the mean. **G** Pressure maps derived from ultrasound modeling were superimposed on the MRI image of one exemplary subject, demonstrating that the focal region of the ultrasound beam successfully overlapped with the intended target regions (GPi and pulvinar). The superimposed modeling shows the axial plane of the subjects' brain, with the intersection of the green lines marking the sonication focal point, informed by subject-specific anatomical data.

Experimental design

Experiment I consisted of three sessions. The initial session involved acquiring MRI images for individual ultrasound modeling, simulations, and neuronavigation during TUS application. The second and third sessions were dedicated to electrophysiology recordings, which were conducted at least one week apart. Figure 1A summarizes the study design and procedures during one electrophysiology recording session. Three out of the 10 patients who had recent pre-existing MRI scans skipped the first session of the experiment. In the first session, the DBS settings of the patients were adjusted to MRI mode before scanning and reverted to their clinical settings upon completion of the MRI session. In visits 2 and 3, an initial neurological assessment was performed by a study neurologist as baseline for safety evaluations. Following this assessment, the DBS device was switched off for the duration of the visit, and 30 min later (following the DBS washout period for LFPs recordings) the LFP recordings started. An example 4-second segment LFP recorded wirelessly is presented in Fig. 1B. Each electrophysiological visit consisted of two parts: initially, a sham procedure (either active or passive), followed by the application of real TUS (tbTUS or 10 Hz TUS) to the GPi of patients who were in the ON-medication state. We employed the NeuroFUS TPO and CTX-500 4-channel transducer (Brainbox Ltd., Cardiff, UK) operating at a central frequency of 500 kHz. For the real TUS protocols of the experiment, we utilized either a theta-burst TUS (tbTUS) protocol[12,51], with parameters of 20 ms pulse duration, 200 ms pulse repetition interval, and 120 s total duration, or a 10 Hz TUS protocol[8,41], with a 30 ms pulse

duration, 100 ms pulse repetition interval, and 40 s total duration. Both protocols were administered bilaterally with an intensity of 30 W/cm² ISPPA (measured in water). The transducer was first positioned on the left side using a neuronavigation system to ensure accurate alignment with the planned target (GPi). After completing the stimulation protocol on the left side, the transducer was repositioned to the right side using the same neuronavigation procedure. Repositioning the transducer, including the neuronavigation steps to ensure accurate targeting, typically took approximately 2 min. The active sham involved targeting a non-motor cortical region, the occipital cortex, with tbTUS protocol with an intensity of 30 W/cm² ISPPA (measured in water), while the passive sham mimicked the actual TUS protocol targeting the GPi, but with an intensity set to 0 W/cm². The application of sham and TUS within each session was necessary due to the two-session limit approved by the University Health Network Research Ethics Board (REB). Given that previous studies have shown tbTUS effects on the motor cortex are short-lived and last about 30 min[12], but the effects on deeper structures such as the GPi are not well understood, we performed sham procedures at the start of each session and real TUS one hour later. This interval served as a washout period for possible residual effects of the active sham condition. LFP recordings were conducted before, during, and after each sonication (10 min, 25 min, and 40 min post-sonication). To minimize potential auditory confound during TUS[70], white noise was played to participants during sonications through earbuds. To account for a comparable timing of dopaminergic medications in PD patients, we scheduled study visits in
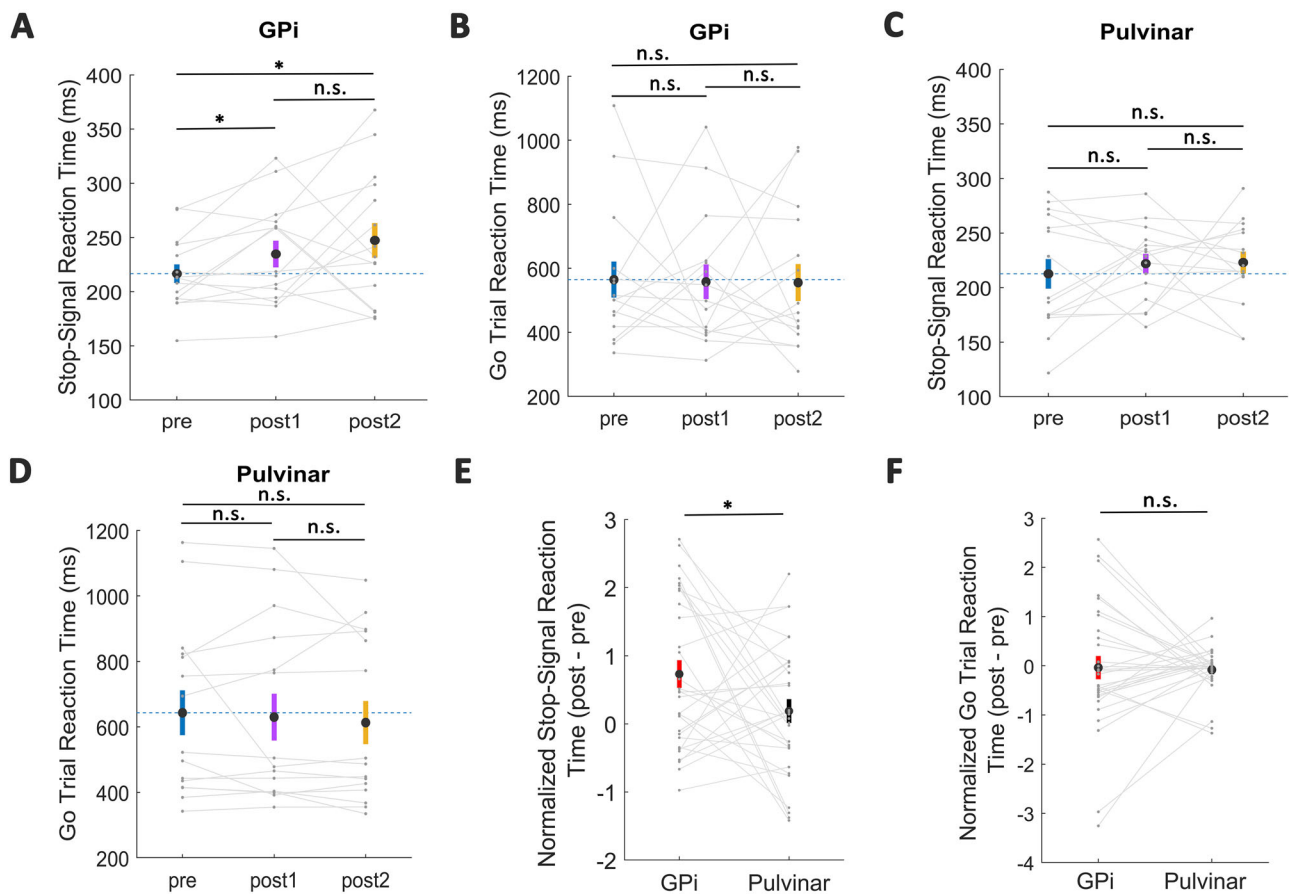
Fig. 9 | Stop-signal task performance pre- and post-intervention in GPi and pulvinar targets. A Stop-signal reaction times (SSRTs) for the GPi target, displayed across three different time points: pre-intervention, post-intervention 1 (post1), and post-intervention 2 (post2). Each data point represents an individual participant's SSRT with group mean marked, demonstrating significantly increased SSRT post-intervention (n = 15 participants; pre vs. post1: p = 0.03, paired t-test; pre vs. post2: p = 0.01, paired t-test; post1 vs. post2: p = 0.45, paired t-test). **B** Go trial reaction times for the GPi target across the same time points as in (**A**), with individual participant data (n = 15) and group mean indicated, showing no significant change (pre vs. post1: p = 0.92, paired t-test; pre vs. post2: p = 0.90, paired t-test; post1 vs. post2: p = 0.97, paired t-test). **C** Stop-signal reaction times for the pulvinar target, with individual participant data (n = 15), displaying no significant change across the time points (pre vs. post1: p = 0.45, paired t-test; pre vs. post2: p = 0.47, paired t-test; post1 vs. post2: p = 0.94, paired t-test). **D** Go trial reaction times for the

pulvinar target, also showing individual participant data (n = 15) without significant differences across the time points (pre vs. post1: p = 0.65, paired t-test; pre vs. post2: p = 0.42, paired t-test; post1 vs. post2: p = 0.49, paired t-test). **E** Comparison of stop-signal reaction times (post - pre) between the two stimulated regions, with individual participant data, displaying significant longer SSRTs when GPi was sonicated (p = 0.04, two-sample t-test). **F** Go trial reaction times did not differ across the two stimulation regions (p = 0.86, two-sample t-test). **E, F** to account for differences in baseline variability between the GPi and pulvinar sessions, post-TUS values were normalized by the standard deviation of the pre-TUS values (n = 30). The asterisk (*) denotes statistically significant differences (p < 0.05), and 'n.s.' indicates non-significant differences. Error bars indicate the standard error of the mean (blue: pre-intervention, purple: post-intervention 1, yellow: post-intervention 2, red: GPi, black: pulvinar).

a way that allowed the experiment to start right after the participants took their medications. The study was designed to be brief, lasting up to 2.5 h. None of the patients were able to distinguish between the sham and real conditions, nor did they report hearing the TUS during the experiments. To minimize biases and placebo effects, we ensured that patients were blinded by providing them with only minimal information about the procedure and steps involved in the study. The order of active vs. passive sham, and 10 Hz vs. tbTUS was randomized across participants. After completion of the LFP recordings, the DBS device was turned back to the patient's usual setting and another neurological assessment was conducted by the study neurologist for safety evaluations.

Lead localization
To assess DBS lead placement, localization was performed using Lead-DBS version 3.0 software (https://www.lead-dbs.org/)[68], in keeping with the previously reported methodology. High-resolution pre- and postoperative T1-weighted 3-dimensional spoiled gradient echo (3D-

SPGR) MRI scans were acquired for each patient. Other acquisition parameters include voxel size = $1 \times 1 \times 1$ mm^3, repetition time (TR) = 9.0/11.9 ms, echo time (TE) = 3.7/5.0 ms, flip angle = 12°/20°). Pre- and postoperative images were linearly registered using SPM12[71] and non-linearly normalized to a Montreal Neurological Institute (MNI) template brain (ICBM 2009b NLIN asymmetric) using ANTs SyN and sub-cortical refinement (http://stnava.github.io/ANTs/)[72]. DBS electrode trajectory was estimated using a semiautomated trajectory reconstruction and manually refined by an experienced user as necessary[73,74]. Since the directionality of the leads was not utilized during the recording sessions, all leads were recreated as omnidirectional.

Local field potentials recording and data analysis
During the second and third sessions of the experiment, LFPs were recorded wirelessly using "Brain Sense Survey Indefinite Streaming" mode in the Medtronic Percept device which streamed to the tablet[75]. Each LFP recording epoch was 4 min long while the patient was at rest,

Table 1 | Patient demographics

Characteristic	Range/Category
Sex	M (n = 9) / F (n = 1)
Age (years)	49–81
Disease Duration (years)	4–34
More Affected Side	Left (n = 5, PD), Right (n = 4, PD), Symmetric (n = 1, Dystonia)
Initial Symptoms	Tremor (n = 3, PD), Reduced Dexterity/Rigidity (n = 6, PD), Dystonic Posture (n = 1, Dystonia)
MDS-UPDRS Score (Med-ON)	13–58
LEDD[a] (mg)	1075–3520

M male, *n* number of patients, *F* female, *PD* Parkinson's Disease, *MDS-UPDRS* Movement Disorder Society Unified Parkinson's Disease Rating Scale, *LEDD* levodopa equivalent daily dose.
[a]Calculated using the following formula and conversion factors: Levodopa equivalent dose calculated as 100 mg of standard levodopa = 133 mg of controlled-release levodopa = 303 mg of entacapone = 100 mg of amantadine = 1 mg of pramipexole =100 mg rasagiline= 5 mg of ropinirole = 3.3 mg of rotigotine = 10 mg of selegiline.

eyes open, and seated comfortably in a chair. Bilateral GPi-LFPs were recorded (bipolar contact pairs: 0-3, 1-3, and 0-2 on one side; and 8-11, 9-11, and 8-10 on the other side) at a sampling rate of 250 Hz and the data recorded from each hemisphere was considered independently for the analysis. This approach is consistent with common practices in electrophysiological studies of the basal ganglia[76–79]. However, we note that treating the hemispheres as independent may carry a risk of inflating effect sizes. LFP data were then extracted via a tablet programmer and stored in a laboratory computer for offline processing. The Percept Toolbox (https://github.com/YohannThenaisie/PerceptToolbox)[80] was used to convert the stored JSON files to.mat files for further analysis in MATLAB (MathWorks, Natick, MA). LFP data were analyzed using MATLAB and the Fieldtrip open-source toolbox, developed at the Donders Institute for Brain, Cognition and Behavior, Radboud University, the Netherlands (https://www.ru.nl/fcdonders/fieldtrip). For preprocessing, 4 min of resting-state LFP data were segmented into 2-s epochs, and 1 Hz fourth-order Butterworth high-pass filtered, followed by 124 Hz low-pass filtering and demeaning. Subsequently, epochs were inspected visually using the summary function of Fieldtrip to remove artifact-contaminated trials. Data were tapered using a Hanning window (bandwidth of smoothing = 2 Hz) and power spectrum density (PSD) estimates in the bandwidth of interest (3–30 Hz) were computed using Fast Fourier Transformation (FFT). PSDs were individually normalized to the total power in the full frequency band of 1–124 Hz. For each patient, the three PSDs from each hemisphere, corresponding to the three bipolar contacts, were averaged prior to comparing the conditions. Significant differences between conditions were assessed using either standard parametric tests (t-test), or nonparametric tests (Wilcoxon signed-rank test, and Mann–Whitney U-test). To assess if the data follows a normal distribution, Lilliefors test was used. Finally, the Benjamini-Hochberg procedure was used to control false discovery (FDR).

Experiment II: Behavioral effects of TUS

Participants. Fifteen healthy participants (age range:18–35 years, average = 23.5, 4 male and 11 female) participated in this experiment. Participants were included if they had no history of neurological, psychological, or medical impairment and were excluded if they were on any medications or drugs. Informed consent was obtained from all participants.

Experimental design. Experiment II consisted of 3 sessions. The initial session involved a brief neurological assessment and acquiring MRI scans. Subsequently, offline simulations and modeling using BabelBrain[42] and Brainsight were conducted to determine the optimal

sonication trajectory. Those participants for whom we had structural MRI scans skipped the first session. In the following two sessions, either the pulvinar or the GPi was targeted bilaterally in random order across participants. The participants first completed a stop-signal task lasting approximately 10–12 min. During the stop-signal task, participants were instructed to fixate on a screen and press the right or left arrow key when a white arrow appeared in the corresponding direction (Go Trial). They were to withhold their response upon seeing a blue arrow after a stop-signal delay (SSD), regardless of direction (Stop Trial). The stop-signal delay (SSD) was adjusted through a staircase procedure, modifying the delay in 50 ms steps in order to achieve roughly 50% successful stops in the Stop trials[81]. The average intertrial interval (ITI) was 2 s. We calculated the stop-signal reaction time (SSRT) for each participant using an integration technique that serves as a measure of inhibitory control effectiveness, as described in (Verbruggen et al., 2019)[81]. Following the stop-signal task, using the simulated data, the location of the transducer on the scalp for neuronavigation (Brainsight, Rogue Research) and the first round of sonication was identified, with the side of the head randomized. To ensure precision, the hair was parted to reveal the scalp, enabling direct placement of the TUS device. Then, adequate ultrasound gel (Wavelength MP Blue, Sabel Med, Oldsmar, FL) was applied to both the participant's head and the transducer, ensuring the absence of air bubbles between the transducer and the scalp, and sonication was delivered for two minutes. In areas where hair density could impede acoustic transmission, the hair was carefully parted, and additional gel was applied to create a continuous and effective coupling layer. We used tbTUS protocol in both sessions at ISPPA of 30 W/cm² (measured in water). After completing sonication to one side, the process was repeated for the contralateral side, only changing the transducer power output (TPO) distance on the TUS device as necessary based on the planned sonication trajectory. Then, participants repeated the stop signal task (post1) before undergoing another round of sonication identical to the first round. Finally, participants performed a third (post2) and final block of the task. It should be noted that the second round of sonication was performed to ensure that tbTUS-induced changes, which have been reported to last up to 30 min[12,51], have not been washed out before enough trials has been collected.

Individualized transcranial acoustic simulations for Experiment I and II

For the planning of TUS applications in both Experiment I and II, we utilized Babelbrain 0.3.0[42], an open-source application that leverages the BabelViscoFDTD library to calculate the acoustic pressure distribution in the brain. In this study, we employed the spatial-peak pulse-average intensity (ISPPA) of 30 W/cm² (measured in water) for all participants, and the corresponding ISPPA at the target location was simulated and reported individually. The selection of ISPPA 30 W/cm², the maximum intensity possible with our transducer, was based on previous published reports of effective TUS in both non-human primates and humans[8,53], safety guidelines, and the consensus of TUS applications by the International Transcranial Ultrasound Safety and Standards (ITRUSST) group[43,44]. In the first visit, participants underwent a T1- and T2-weighted three-dimensional MR-image on a Siemens Magnetom Prisma scanner. The parameters for the T1-weighted images were as follows: repetition time (TR) = 2400.0 ms, echo time (TE) = 3.69 ms, inversion time (TI) = 962 ms, flip angle = 8 degrees, field of view (FOV) = 256 mm, slice thickness = 1.0 mm isotropic, number of slices = 176 and acquisition time = 10 min 16 s. For the T2-weighted image, the parameters were: TR = 7000 ms, TE = 428 ms, an echo train length of 248 ms, FOV = 256 mm, slice thickness = 1.0 mm, and an acceleration factor of 2 using CAIPI, and acquisition time = 8 min 40 s. Using neuronavigation software, Brainsight (Rogue Research), targets were identified on T1w images at DBS lead contacts 1 and 9 (first and second lead) for each patient individually in **Experiment I**. In

Experiment II, Using Advanced Normalization Tools (ANTs), MRIs were non-linearly transformed into the standard Montreal Neurological Institute (MNI) space. The transformations obtained were then applied to the sonication target coordinates to map them from MNI space to the native MRI space. The MNI coordinates, taken from the AAL3 atlas, for the GPi and pulvinar were x, y, z = (±20, −8, −4), and x, y, z = (±11, −33, 6) respectively. These coordinates were then fine-tuned to ensure precise alignment with the target region based on the participant's individual MRI anatomy. The fine-tuned coordinates were then transferred to the neuronavigation software (Brainsight, Rogue Research, Canada). An initial targeting trajectory, perpendicular to the temporal bone, was determined to minimize the distance from the bone to the target while avoiding the optic tract for each patient individually. This trajectory represents a vector indicating the transducer's focus position and acoustic axis alignment in T1w space. NifTI files of the participant's 3-D isotropic 1 mm resolution T1w scans, along with NifTI files of segmented tissue, were uploaded into Babelbrain. The segmented tissue was derived using SimNIBS 4.0 charm processing tool, based on participants' T1w and T2w scans. Utilizing masks overlaid on the segmented tissue, BabelBrain estimated the transmitted acoustic field and thermal rise in the brain tissue, accounting for skull distortions (Fig. 2A, B). Thermal effects were modeled by solving the Bio Heat Thermal Equation[82,83]. Table S3 summarizes the physical parameters used for acoustic and thermal modeling. For thermal simulations, the 10 Hz TUS protocol included 40 s of sonication with a 30% duty cycle, while the tbTUS protocol included 120 s with a 10% duty cycle as input parameters. It is worth noting that, because this was a single exposure, the ISPTA is just the product of ISPPA and DC. The spatial resolution for simulations was set to 6 points-per-wavelength (PPW) in water conditions with an ultrasound frequency of 500 kHz.

The transducer was calibrated with optical trackers for live tracking before each session. Subsequently, the optimal trajectory estimated in BabelBrain was employed for transducer placement on the scalp, continuously monitoring of the transducer location relative to the target with our neuronavigation system online. Therefore, this optimal trajectory accounts for beam deviation due to skull geometry and maximizes the probability of engaging the stimulation targets (DBS-lead contact in the GPi in Experiment I and the GPi and pulvinar in Experiment II). All BabelBrain modeling was conducted on a M1 Max MacBook Pro system with 64 B RAM, running OSX 14.2.1.

Free field acoustic simulations

A three-dimensional simulation of the acoustic pressure field, as it propagates through water, was also performed using Babelbrain software. The acoustic pressure distribution in water at an ISPPA of 30 W/cm^2 for a focal depth of 60 mm, which represents the right GPi depth for one of the patients, is shown in Fig. S1. The full width at half maximum (FWHM), important for determining the spatial resolution of the TUS, was 27 mm along the trajectory, and the lateral cross-section of the beam was 4.7 mm. The -6dB length and diameter of the elliptical focal spot in situ were 24.33 ± 3.63 mm (mean ± std) and 4.3 ± 0.5 mm (mean ± std), respectively. The focal spot dimensions which are simulated are all in full agreement with the experimental water tank measurements provided by the manufacturer (SonicConcepts, WA, USA).

Reporting summary

Further information on research design is available in the Nature Portfolio Reporting Summary linked to this article.

Data availability

All behavioral data from healthy participants and the acoustic simulation data are publicly available at Figshare (https://figshare.com/s/359031a0ea6613016a8b). Upon request, the de-identified local field potential data from individual patients will be made available to investigators by the corresponding authors via private online cloud storage. Source data are provided with this paper.

References

1. Darmani, G. et al. Non-invasive transcranial ultrasound stimulation for neuromodulation. *Clin. Neurophysiol.* **135**, 51–73 (2022).
2. Wagner, T., Valero-Cabre, A. & Pascual-Leone, A. Noninvasive human brain stimulation. *Annu. Rev. Biomed. Eng.* **9**, 527–565 (2007).
3. Lozano, A. M. et al. Deep brain stimulation: current challenges and future directions. *Nat. Rev. Neurol.* **15**, 148–160 (2019).
4. Folloni, D. et al. Manipulation of subcortical and deep cortical activity in the primate brain using transcranial focused ultrasound stimulation. *Neuron* **101**, 1109–1116.e5 (2019).
5. Kubanek, J. et al. Remote, brain region–specific control of choice behavior with ultrasonic waves. *Sci. Adv.* **6**, eaaz4193 (2020).
6. Legon, W. et al. Transcranial focused ultrasound modulates the activity of primary somatosensory cortex in humans. *Nat. Neurosci.* **17**, 322–329 (2014).
7. Tyler, W. J. et al. Remote excitation of neuronal circuits using low-intensity, low-frequency ultrasound. *PLOS ONE* **3**, e3511 (2008).
8. Verhagen, L. et al. Offline impact of transcranial focused ultrasound on cortical activation in primates. *Elife* **8**, e40541 (2019).
9. Yang, P. S. et al. Transcranial focused ultrasound to the thalamus is associated with reduced extracellular GABA levels in rats. *Neuropsychobiology* **65**, 153–160 (2012).
10. Yoo, S., Mittelstein, D. R., Hurt, R. C., Lacroix, J. & Shapiro, M. G. Focused ultrasound excites cortical neurons via mechanosensitive calcium accumulation and ion channel amplification. *Nat. Commun.* **13**, 493 (2022).
11. Yu, K., Niu, X., Krook-Magnuson, E. & He, B. Intrinsic functional neuron-type selectivity of transcranial focused ultrasound neuromodulation. *Nat. Commun.* **12**, 2519 (2021).
12. Zeng, K. et al. Induction of human motor cortex plasticity by theta burst transcranial ultrasound stimulation. *Ann. Neurol.* **91**, 238–252 (2022).
13. Gulick, D. W., Li, T., Kleim, J. A. & Towe, B. C. Comparison of electrical and ultrasound neurostimulation in rat motor cortex. *Ultrasound Med. Biol.* **43**, 2824–2833 (2017).
14. Kamimura, H. A. S. et al. Focused ultrasound neuromodulation of cortical and subcortical brain structures using 1.9 MHz. *Med. Phys.* **43**, 5730–5735 (2016).
15. King, R. L., Brown, J. R., Newsome, W. T. & Pauly, K. B. Effective parameters for ultrasound-induced in vivo neurostimulation. *Ultrasound Med. Biol.* **39**, 312–331 (2013).
16. Tufail, Y. et al. Transcranial pulsed ultrasound stimulates intact brain circuits. *Neuron* **66**, 681–694 (2010).
17. Kim, H., Chiu, A., Lee, S. D., Fischer, K. & Yoo, S.-S. Focused ultrasound-mediated non-invasive brain stimulation: examination of sonication parameters. *Brain Stimul.* **7**, 748–756 (2014).
18. Kim, H.-J. et al. Long-lasting forms of plasticity through patterned ultrasound-induced brainwave entrainment. *Sci. Adv.* **10**, eadk3198 (2024).
19. Murphy, K. R. et al. A tool for monitoring cell type-specific focused ultrasound neuromodulation and control of chronic epilepsy. *Proc. Natl. Acad. Sci. USA* **119**, e2206828119 (2022).
20. Wang, Z., Yan, J., Wang, X., Yuan, Y. & Li, X. Transcranial ultrasound stimulation directly influences the cortical excitability of the motor cortex in parkinsonian mice. *Mov. Disord.* **35**, 693–698 (2020).
21. Li, X. et al. Seizure control by low-intensity ultrasound in mice with temporal lobe epilepsy. *Epilepsy Res.* **154**, 1–7 (2019).
22. Samuel, N. et al. Accelerated transcranial ultrasound neuromodulation in Parkinson's Disease: a pilot study. *Mov. Disord.* **38**, 2209–2216 (2023).

23. Sarica, C. et al. Human studies of transcranial ultrasound neuro-modulation: a systematic review of effectiveness and safety. *Brain Stimul.* **15**, 737–746 (2022).

24. Bubrick, E. J. et al. Transcranial ultrasound neuromodulation for epilepsy: a pilot safety trial. *Brain Stimul.* **17**, 7–9 (2024).

25. Monti, M. M., Schnakers, C., Korb, A. S., Bystritsky, A. & Vespa, P. M. Non-invasive ultrasonic thalamic stimulation in disorders of consciousness after severe brain injury: a first-in-man report. *Brain Stimulat.* **9**, 940–941 (2016).

26. Grippe, T. et al. Plasticity-induced effects of theta burst transcranial ultrasound stimulation in parkinson's disease. *Mov. Disord.* https://doi.org/10.1002/mds.29836 (2024).

27. Prieto, M. L., Ömer, O., Khuri-Yakub, B. T. & Maduke, M. C. Dynamic response of model lipid membranes to ultrasonic radiation force. *PloS ONE* **8**, e77115 (2013).

28. Gaub, B. M. et al. Neurons differentiate magnitude and location of mechanical stimuli. *Proc. Natl. Acad. Sci. USA* **117**, 848–856 (2020).

29. Chen, H., Garcia-Gonzalez, D. & Jérusalem, A. Computational model of the mechanoelectrophysiological coupling in axons with application to neuromodulation. *Phys. Rev. E* **99**, 032406 (2019).

30. Hoffman, B. U. et al. Focused ultrasound excites action potentials in mammalian peripheral neurons in part through the mechanically gated ion channel PIEZO2. *Proc. Natl. Acad. Sci. USA* **119**, e2115821119 (2022).

31. Qiu, Z. et al. The mechanosensitive ion channel Piezo1 significantly mediates in vitro ultrasonic stimulation of neurons. *iScience* **21**, 448–457 (2019).

32. Prieto, M. L., Firouzi, K., Khuri-Yakub, B. T. & Maduke, M. Activation of Piezo1 but Not NaV1.2 channels by ultrasound at 43 MHz. *Ultrasound Med. Biol.* **44**, 1217–1232 (2018).

33. Kubanek, J. et al. Ultrasound modulates ion channel currents. *Sci. Rep.* **6**, 24170 (2016).

34. Oh, S.-J. et al. Ultrasonic Neuromodulation via Astrocytic TRPA1. *Curr. Biol.* **29**, 3386–3401.e8 (2019).

35. Barnett, S. B., Rott, H. D., ter Haar, G. R., Ziskin, M. C. & Maeda, K. The sensitivity of biological tissue to ultrasound. *Ultrasound Med. Biol.* **23**, 805–812 (1997).

36. Kamimura, H. A. S., Conti, A., Toschi, N. & Konofagou, E. E. Ultrasound neuromodulation: mechanisms and the potential of multi-modal stimulation for neuronal function assessment. *Front. Phys.* **8**, 150 (2020).

37. McGregor, M. M. & Nelson, A. B. Circuit Mechanisms of Parkinson's Disease. *Neuron* **101**, 1042–1056 (2019).

38. Hammond, C., Bergman, H. & Brown, P. Pathological synchronization in Parkinson's disease: networks, models and treatments. *Trends Neurosci.* **30**, 357–364 (2007).

39. Jirsch, J. D. et al. High-frequency oscillations during human focal seizures. *Brain J. Neurol.* **129**, 1593–1608 (2006).

40. Sarica, C. et al. Toward focused ultrasound neuromodulation in deep brain stimulator implanted patients: ex-vivo thermal, kinetic and targeting feasibility assessment. *Brain Stimulat.* **15**, 376–379 (2022).

41. Nakajima, K. et al. A causal role of anterior prefrontal-putamen circuit for response inhibition revealed by transcranial ultrasound stimulation in humans. *Cell Rep.* **40**, 111197 (2022).

42. Pichardo, S. BabelBrain: an Open-Source application for prospective modeling of transcranial focused ultrasound for neuromodulation applications. *IEEE Trans. Ultrason. Ferroelectr. Freq. Control* **70**, 587–599 (2023).

43. Marketing Clearance of Diagnostic Ultrasound Systems and Transducers. *Guidance for Industry and Food and Drug Administration Staff.* Permanent Link at https://resource.nlm.nih.gov/101760255 (US Food and Drug Adminstration, MD, USA, 2019).

44. Aubry, J.-F. et al. ITRUSST consensus on biophysical safety for transcranial ultrasonic stimulation. Preprint at http://arxiv.org/abs/2311.05359 (2023).

45. Silberstein, P. et al. Patterning of globus pallidus local field potentials differs between Parkinson's disease and dystonia. *Brain J. Neurol.* **126**, 2597–2608 (2003).

46. Neumann, W.-J., Feldmann, L. & Kühn, A. A. Reply to: pallidal low-frequency activity in dystonia and subthalamic beta activity in Parkinson's Disease. *Mov. Disord.* **35**, 1699 (2020).

47. Scheller, U. et al. Pallidal low-frequency activity in dystonia after cessation of long-term deep brain stimulation. *Mov. Disord.* **34**, 1734–1739 (2019).

48. Tsang, E. W. et al. Prominent 5-18 Hz oscillations in the pallidal-thalamic circuit in secondary dystonia. *Neurology* **78**, 361–363 (2012).

49. Tsang, E. W. et al. Movement related potentials and oscillatory activities in the human internal globus pallidus during voluntary movements. *J. Neurol. Neurosurg. Psychiatry* **83**, 91–97 (2012).

50. Shamli Oghli, Y. et al. Mechanisms of theta burst transcranial ultrasound induced plasticity in the human motor cortex. *Brain Stimulat.* **16**, 1135–1143 (2023).

51. Zeng, K. et al. Effects of different sonication parameters of theta burst transcranial ultrasound stimulation on human motor cortex. *Brain Stimulat.* **17**, 258–268 (2024).

52. Zadeh, A. K. et al. The effect of transcranial ultrasound pulse repetition frequency on sustained inhibition in the human primary motor cortex: a double-blind, sham-controlled study. *Brain Stimulat.* **17**, 476–484 (2024).

53. Yaakub, S. N. et al. Transcranial focused ultrasound-mediated neurochemical and functional connectivity changes in deep cortical regions in humans. *Nat. Commun.* **14**, 5318 (2023).

54. Chaplin, V. et al. On the accuracy of optically tracked transducers for image-guided transcranial ultrasound. *Int. J. Comput. Assist. Radiol. Surg.* **14**, 1317–1327 (2019).

55. Xu, L. et al. Characterization of the targeting accuracy of a neuronavigation-guided transcranial FUS system in vitro, in vivo, and in silico. *IEEE Trans. Biomed. Eng.* **70**, 1528–1538 (2023).

56. Wu, S.-Y. et al. Efficient blood-brain barrier opening in primates with neuronavigation-guided ultrasound and real-time acoustic mapping. *Sci. Rep.* **8**, 7978 (2018).

57. Riis, T. S., Losser, A. J., Kassavetis, P., Moretti, P. & Kubanek, J. Noninvasive modulation of essential tremor with focused ultrasonic waves. *J. Neural Eng.* **21**, 016033 (2024).

58. Kusunose, J. et al. Design and validation of a patient-specific stereotactic frame for transcranial ultrasound therapy. *IEEE Trans. Ultrason. Ferroelectr. Freq. Control* **71**, 1030–1041 (2024).

59. Min, B.-K. et al. Focused ultrasound modulates the level of cortical neurotransmitters: potential as a new functional brain mapping technique. *Int. J. Imaging Syst. Technol.* **21**, 232–240 (2011).

60. Brown, P. et al. Dopamine dependency of oscillations between subthalamic nucleus and pallidum in Parkinson's disease. *J. Neurosci.* **21**, 1033–1038 (2001).

61. Yin, Z. et al. Local field potentials in Parkinson's disease: a frequency-based review. *Neurobiol. Dis.* **155**, 105372 (2021).

62. Foffani, G. et al. Altered subthalamo-pallidal synchronisation in parkinsonian dyskinesias. *J. Neurol. Neurosurg. Psychiatry* **76**, 426–428 (2005).

63. Martin, E. et al. Ultrasound system for precise neuromodulation of human deep brain circuits. Preprint at https://doi.org/10.1101/2024.06.08.597305 (2024).

64. Badran, B. W. et al. Sonication of the anterior thalamus with MRI-Guided transcranial focused ultrasound (tFUS) alters pain thresholds in healthy adults: A double-blind, sham-controlled study. *Brain Stimulat.* **13**, 1805–1812 (2020).

65. Criaud, M. et al. The human basal ganglia mediate the interplay between reactive and proactive control of response through both motor inhibition and sensory modulation. *Brain Sci.* **11**, 560 (2021).

66. Li, C. R., Yan, P., Sinha, R. & Lee, T.-W. Sub-cortical processes of motor response inhibition during a stop signal task. *NeuroImage* **41**, 1352–1363 (2008).

67. Frank, M. J., Samanta, J., Moustafa, A. A. & Sherman, S. J. Hold your horses: impulsivity, deep brain stimulation, and medication in parkinsonism. *Science* **318**, 1309–1312 (2007).

68. Horn, A. & Kühn, A. A. Lead-DBS: a toolbox for deep brain stimulation electrode localizations and visualizations. *NeuroImage* **107**, 127–135 (2015).

69. Sarica, C. et al. Trends and disparities in deep brain stimulation utilization in the United States: a Nationwide Inpatient Sample analysis from 1993 to 2017. *Lancet Reg. Health Am.* **26**, 100599 (2023).

70. Kop, B. R. et al. Auditory confounds can drive online effects of transcranial ultrasonic stimulation in humans. *Elife.* **12**, RP88762 (2024).

71. Penny, W. D., Friston, K. J., Ashburner, J. T., Kiebel, S. J. & Nichols, T. E. *Statistical Parametric Mapping: The Analysis of Functional Brain Images* (Elsevier, 2011).

72. Avants, B. B. et al. A reproducible evaluation of ANTs similarity metric performance in brain image registration. *NeuroImage* **54**, 2033–2044 (2011).

73. Astrom, M., Diczfalusy, E., Martens, H. & Wardell, K. Relationship between neural activation and electric field distribution during deep brain stimulation. *IEEE Trans. Biomed. Eng.* **62**, 664–672 (2015).

74. McIntyre, C. C., Mori, S., Sherman, D. L., Thakor, N. V. & Vitek, J. L. Electric field and stimulating influence generated by deep brain stimulation of the subthalamic nucleus. *Clin. Neurophysiol.* **115**, 589–595 (2004).

75. Sanger, Z. T. et al. Neural signal data collection and analysis of Percept™ PC BrainSense recordings for thalamic stimulation in epilepsy. *J. Neural Eng.* **21**, 012001 (2024).

76. Strelow, J. N. et al. Local field potential-guided contact selection using chronically implanted sensing devices for deep brain stimulation in Parkinson's Disease. *Brain Sci.* **12**, 1726 (2022).

77. Johnson, K. A. et al. Globus pallidus internus deep brain stimulation evokes resonant neural activity in Parkinson's disease. *Brain Commun.* **5**, fcad025 (2023).

78. Trenado, C. et al. Local field potential oscillations of the globus pallidus in cervical and tardive dystonia. *J. Neurol. Sci.* **366**, 68–73 (2016).

79. Swinnen, B. E. K. S. et al. Clinically implemented sensing-based initial programming of deep brain stimulation for Parkinson's Disease: a retrospective study. *Neuromodulation*. 1–10 (2024).

80. Thenaisie, Y. et al. Towards adaptive deep brain stimulation: clinical and technical notes on a novel commercial device for chronic brain sensing. *J. Neural Eng.* **18**, 042002 (2021).

81. Verbruggen, F. et al. A consensus guide to capturing the ability to inhibit actions and impulsive behaviors in the stop-signal task. *eLife* **8**, e46323 (2019).

82. Sapareto, S. A. & Dewey, W. C. Thermal dose determination in cancer therapy. *Int. J. Radiat. Oncol. Biol. Phys.* **10**, 787–800 (1984).

83. Baumgartner, C. et al. IT'IS database for thermal and electro-magnetic parameters of biological tissues, Version 4.2. IT'IS Foundation https://doi.org/10.13099/VIP21000-04-2 (2024).

Acknowledgements

Author contributions

G.D.: conceptualization, experimental design and set up, data acquisition, analysis, data interpretation, manuscript writing. H.R.: conceptualization, experimental design and set up, analysis, data interpretation, manuscript writing. C.S.: conceptualization, experimental design and set up, data acquisition, data interpretation, manuscript edits. RA: experimental set up, data acquisition, data interpretation, manuscript edits. T.G., J.F.N., A.F., B.S., K.Z., A.V., N.S., B.D., A.F., M.L., and S.K.: data acquisition, data interpretation, manuscript edits. S.P.: experimental set up, analysis, data interpretation, manuscript edits. AML: conceptualization, data interpretation, manuscript edits, supervision and funding. R.C.: conceptualization, experimental design, data interpretation, manuscript edits, supervision and funding.

Competing interests

The authors declare no competing interests.

Additional information

Supplementary information The online version contains supplementary material available at https://doi.org/10.1038/s41467-025-57883-7.

Correspondence and requests for materials should be addressed to Ghazaleh Darmani or Robert Chen.

Peer review information *Nature Communications* thanks Nanditha Rajamani, who co-reviewed with Patricia Zvarovaand the other, anonymous, reviewers for their contribution to the peer review of this work. A peer review file is available.

Reprints and permissions information is available at http://www.nature.com/reprints

Publisher's note Springer Nature remains neutral with regard to jurisdictional claims in published maps and institutional affiliations.